Title
BACKWARD NEUTRON-PROTON SCATTERING WITH A POLARIZED TARGET

Author
Robrish, Peter Ronald.

Publication Date
1972-08-01

BACKWARD NEUTRON-PROTON SCATTERING WITH A POLARIZED TARGET

Peter Ronald Robrish
(Ph.D. Thesis)

August 1972

AEC Contract No. W-7405-eng-48

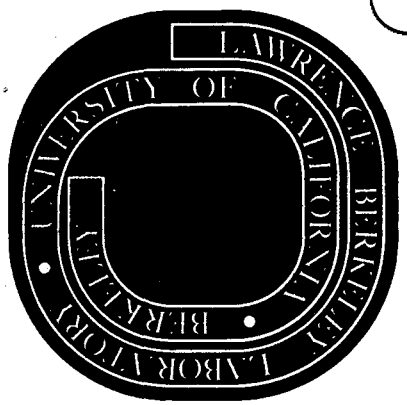

DISCLAIMER

BACKWARD NEUTRON-PROTON SCATTERING WITH A POLARIZED TARGET

Contents

BACKWARD NEUTRON-PROTON SCATTERING WITH A POLARIZED TARGET

Peter Ronald Robrish

Lawrence Berkeley Laboratory
University of California
Berkeley, California 94720

August 1972

Abstract

This thesis presents a description of an experiment which measured the asymmetry in the elastic scattering of neutrons from polarized protons, for incident neutron momenta of from 1.0 to 5.5 GeV/c and for final neutron scattering angles near 180° in the center-of-mass. The angles considered in the experiment correspond to a momentum transfer range of $0 \leq -u \leq .6$ and within this range the asymmetry was consistently negative (where the normal to the scattering plane is defined by the cross product of the initial and final neutron momentum vectors). The asymmetry could be reasonably represented by a function of the form $A(-u) = -(1/2M_p)\sqrt{-u}$ where M_p is the mass of the proton.

I. INTRODUCTION

In this paper I discuss a measurement of the asymmetry of neutrons elastically scattered from polarized protons with scattering angles near 180° in the center-of-mass system. The asymmetry is equivalent to the polarization parameter (i.e. the recoil nucleon polarization found in the scattering of an unpolarized beam from an unpolarized target) if parity and time reversal are good symmetries in this process (I will often be sloppy and call this a measurement of the polarization). This measurement is another small addition to the already voluminous literature concerned with the nucleon-nucleon problem. This larger problem has always been a central one for study in high energy physics. Whether it should be a central problem for work is, I think, a question to which too little attention has been paid. Nucleon-nucleon scattering has been studied extensively because beams and targets of nucleons are readily available. It is certainly possible that some other system, for example the $\pi\pi$ system, might do for strong-interaction theory what the hydrogen atom did for atomic theory. However, since we are experimentally limited to studying only certain systems we choose to study a particular reaction because of the anomalies observed in that reaction.

Backward np scattering[1] at high energies (greater than 1 GeV) has only recently received much experimental and theoretical attention. The impetus for this attention is the anomalous behavior of the differential cross section near 180°, which I will discuss in more detail in the next section. There have been many attempts to explain the behavior of

the cross section, but only those using a large number of free parameters have had anything like reasonable success. We undertook this experiment hoping to further constrain the theoretical models for this process.

In order to perform the measurement we bombarded a polarized-proton target with a neutron beam having a broad spectrum of momenta from 1 to 5.5 GeV/c. We determined the direction and momentum of protons emerging from the target near the forward direction by using a magnetic spectrometer. An array of neutron counters was used to measure the direction of the outgoing neutron and its velocity. By measuring both the velocity of the neutron and the angular correlation between the directions of the outgoing neutron and proton, we were able to determine whether a given event was elastic scattering from the free hydrogen in the target. For such an event we used the measured momentum and direction of the outgoing proton to calculate the momentum of the incident neutron.

The asymmetry A(u) is defined so that for a target of polarization $\vec{P}_T$ the intensity at a given momentum transfer I(u) is given by

$$I(u) = I_0(u) \ (1 + A(u) \ \vec{P}_T \cdot \hat{n})$$

where $I_0(u)$ is the ordinary differential cross section and $\hat{n}$ is the normal to the scattering plane. We have chosen to define $\hat{n}$ as in the direction of the vector product $\vec{K}_i \times \vec{K}_f$ of the incident and scattered neutron momenta and correspondingly to define the charge exchange momentum transfer variable as u (u is the Mandelstam variable which goes to zero

at a center-of-mass scattering angle of 180° for equal mass scattering--we will ignore the np mass difference in all discussion). These are not usual conventions for those who like to think of this reaction as forward charge-exchange scattering, but we chose it for the convenience of anyone who measures the asymmetry for both forward and backward np scattering.

In principle one need only measure I(u) for one sign of polarization but in practice one measures I_+ and I_- (corresponding to $\vec{P}_T \cdot \hat{n} = \pm |P_T|$) so that one need not know I_0 and can minimize the effect of background. A(u) is then simply related to I_+ and I_- (assuming $|P_T^+| = |P_T^-|$) by

$$A(u) = \frac{1}{|P_T|} \frac{I_+ - I_-}{I_+ + I_-}$$

In the actual experiment, $|P_T|$ is not always the same and there is a background caused by scattering from unpolarized nuclei that contributes to I_+ and I_-. We will discuss these points later. The measurement is made by determining the intensity of elastic scattering at fixed angles for both signs of polarization. From these data one calculates the asymmetry.

II. SUMMARY OF PREVIOUS WORK IN BACKWARD np SCATTERING

A. Experiments

The reaction np → pn elastic scattering near 180° in the center-of-mass (c.m.) is often referred to as np charge-exchange scattering, mainly because theoretical work in the problem has tended to concentrate on viewing it as a process controlled by a diagram like Fig. 1, where X is some charged particle. Previous experiments concerned with this reaction have concentrated on measuring the differential cross section $d\sigma/du$.

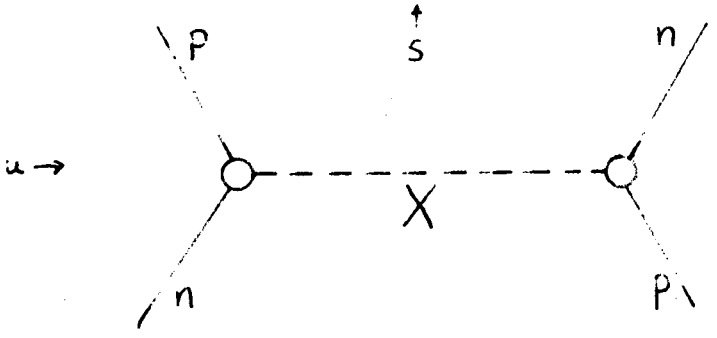

Fig. 1. Single Particle Exchange Diagram for np → pn.

The most recent experiments [2,3,4,5] which have measured this reaction at high energies (above 1 BeV/c incident neutron momenta) have all observed the same general features. The cross section has a very sharp peak near u = 0 and rather suddenly flattens out at about u = -0.02. The cross section can be fitted quite well by a function of the form:

$$\frac{d\sigma}{du} = (Ae^{\alpha u} + Be^{\beta u}) \left.\frac{d\sigma}{du}\right|_{u=0} \qquad (1)$$

where α is of the order of 60 and β of the order of 5. The parameters A, B, α, β do not show much variation with energy at high energies. Wilson[6] has pointed out that this sharp peak near u = 0 persists at energies as low as 90 MeV (430 MeV/c), though recent measurements[4] have shown that there is more energy dependence in the parameters of (1) at low energies than there is at energies above 1 GeV. The sharpness of this backward peak is quite striking when compared with the forward peak of a process like pp scattering where the diffraction peak goes like e^{10t}. The only comparable peaking occurs in the photoproduction of charged pions,[7] and models which attempt to deal with that reaction have the same difficulties as those dealing with np → pn.

There have been two measurements[8,9] of the asymmetry in np scattering at momenta near the lowest which we considered in the present experiment (1 GeV/c). Both measurements were double scattering experiments in which the beam (of protons) was first polarized by scattering, and then allowed to scatter from the neutrons in a deuterium target. The asymmetry was obtained by measuring the difference in counting rate for elastic scattering at a fixed angle when the polarization of the beam was reversed. Both of these expriments covered a large angular region, and both were designed with the objective of helping to pin down the nucleon-nucleon phase shifts at intermediate energies. The present experiment concentrates on a higher energy region and on angles very near the backward direction. Our hope was to further constrain the

high energy theories which were already having difficulty explaining the differential cross-section data.

B. Theoretical Models of High Energy np Backward Scattering

The starting point for theoretical work on this problem is the notion that the exchange of a π meson provides the mechanism for the rapid variation of the cross section near $u = 0$. In diffractive scattering, the sharpness of the diffraction peak corresponds to the size of the object which did the scattering, or, alternatively, to the range of the force which controlled the interaction. A sharp peak indicates a long range force. If we consider the strong interactions to be forces generated by the exchange of particles, then only the pion has a small enough mass to be responsible for the long-range force which gives rise to the sharp peak in np scattering. So far, it appears that we really have a fine solution to the problem; however, this solution suffers from a rather annoying disease. The disease may be illustrated most transparently if we write down a typical scattering amplitude for the process in the Born approximation. We suppose the amplitude to be that generated by the exchange of a single pion. The amplitude is then proportional to

$$\frac{u}{u - m_\pi^2}$$

and the problem is manifest, since such an amplitude obviously vanishes at $u = 0$. All theoretical models which attempt to deal with this process must get around this initial stumbling block.

The most naive approach to the problem is to note that

$$\frac{u}{u - m_\pi^2} = 1 + \frac{m_\pi^2}{u - m_\pi^2}$$

and that the first term, which contributes to s-wave scattering, leads to a violation of the unitarity limit as the energy increases. If we can get rid of the 1, that is the term in the amplitude which does not depend on u, then we have an amplitude which leads to a peak in the cross section at u = 0. The essence of the absorptive correction to the Born approximation is that there is a background amplitude which interferes destructively with the Born amplitude and which varies slowly with momentum transfer, thus cancelling the constant part of that amplitude. Models which used only one-pion exchange plus a phenomenological absorptive correction were able to reproduce the forward peak, however, they also predict a secondary maximum which is not seen.[10]

Byers[11] has considered this reaction using a coherent droplet model with one-pion exchange. In essence this model gets rid of the anomalous s-wave part of the Born amplitude by ignoring it. The contributions to the scattering amplitude from low partial waves are given by an eikonal representation. One supposes that the backward amplitude is proportional to the absorptive part of the forward elastic scattering amplitude. In the eikonal approximation the partial-wave summation is replaced by a suitable integral over an impact parameter, and the elastic scattering phase shift is considered to be a continuous function of this parameter. This function is found by fitting the forward elastic-scattering data. The constants of proportionality are then adjusted to fit the backward cross-section data. This droplet representation is used for small impact parameters, and is constrained to reduce

to the eikonal representation for single-pion exchange at large impact parameters. The model seems to fit the np → pn reaction and the crossed channel pp → nn reaction quite well; however there is still a good deal of freedom in the parameters of the model which would be further constrained only by measurements of some of the spin-dependent effects.

Next I would like to consider Regge Models for np → pn, but before I do, I had better discuss in some detail the amplitudes involved in nucleon-nucleon scattering, since I will have to deal with these amplitudes more specifically in order to try to explain the ways in which Regge Models attempt to get around the problems inherent in the description of np backward scattering. For each isospin state there are five independent amplitudes. This can be shown by taking the sixteen possible amplitudes constructed from the various spin combinations in the initial and final state and using P and T invariance along with the Pauli principle. One can express these five amplitudes with respect to various representations of the spin states, but the one usually used is the helicity representation of Jacob and Wick.[12] In this representation the axis of quantization for the spins of each of the nucleons is their respective momentum directions. The five independent s-channel helicity amplitudes are then[13]

$$\phi_1 = \langle + + | \phi_1 | + + \rangle$$
$$\phi_2 = \langle + + | \phi_2 | - - \rangle$$
$$\phi_3 = \langle + - | \phi_3 | + - \rangle$$
$$\phi_4 = \langle + - | \phi_4 | - + \rangle$$
$$\phi_5 = \langle + + | \phi_5 | + - \rangle$$

where the + (-) indicates that the particle has its spin parallel (anti-parallel) to its direction of motion. ϕ_3 and ϕ_5 must vanish in the backward direction since angular momentum is conserved. If one looks at the partial wave expansions of ϕ_3 and ϕ_5, it is easy to see that near $u = 0$ ϕ_3 is proportional to u and ϕ_5 to $\sqrt{-u}$.

Using these amplitudes, the cross section as a function of center-of-mass angle may be written:

$$I_0(\theta) = \frac{1}{2}\left(|\phi_1|^2 + |\phi_2|^2 + |\phi_3|^2 + |\phi_4|^2 + 4|\phi_5|^2\right)$$

and the polarization parameter $P(\theta)$ and the asymmetry $A(\theta)$ (assuming P and T invariance) can be obtained from

$$I_0 A(\theta) = I_0 P(\theta) = \text{Im}\ \phi_5(\phi_1 + \phi_2 + \phi_3 - \phi_4)^* \quad .$$

Now with this brief digression we are ready to consider the Regge approach to the problem.

Muzinich[14] has discussed the nucleon-nucleon problem in general using the Regge pole model. In $np \to pn$, the Regge trajectories which are involved in exchanges in the u channel must be associated with isovector mesons. The trajectories which are supposed to play a dominant role in this process are the ρ, A_2, and π. The ρ and A_2 contribute because they are the highest lying trajectories, and the π is brought in because it has a pole so near the physical region (this is another way of saying that it has a small mass and therefore must contribute to the long-range force which causes the sharp forward peak). Muzinich shows that the π trajectory contributes only to ϕ_2 and ϕ_3, and that it contributes in such a way that $\phi_2^\pi = -\phi_3^\pi$. The ρ and A_2 trajectories contribute to all of the amplitudes (at large energies $\phi_1^{\rho,A_2} = -\phi_4^{\rho,A_2}$ and $\phi_2^{\rho,A_2} = \phi_3^{\rho,A_2}$ for

these trajectories). While these three trajectories are supposed to dominate the description of the reaction at high energies and small u, most fits to the data bring in other trajectories in order to have enough flexibility to get a successful fit at a number of different energies.

The basic problem encountered in Regge fits to the data is the same as that found in the early single-pion-exchange models. Recall that the amplitude ϕ_3 must vanish at u = 0. The contributions of the ρ and A_2 trajectories to ϕ_3 vary with energy like $s^{\alpha_\rho(u)}$ and $s^{\alpha_{A_2}(u)}$ respectively, while the contribution of the π varies like $s^{\alpha_\pi(u)}$. The functions $\alpha(u)$ are the trajectory functions associated with the Regge trajectories. Since $\alpha_\pi(0)$ is very different from $\alpha_\rho(0)$ and $\alpha_{A_2}(0)$, the contributions of the ρ and A_2 trajectories to ϕ_3 could, at best, cancel that of the π at only one value of the total energy. Since ϕ_3 must vanish at u = 0 for all energies, each of the contributions to ϕ_3 must vanish separately. Therefore, since $\phi_3^\pi = -\phi_2^\pi$, the pion will contribute nothing to the cross section at u = 0, and we are right back where we were before. The ρ and A_2 contributions to the cross section vary rather slowly as u goes away from zero, and the rapid variation of the pion contribution will produce a dip, not the peak required, at u = 0. In order to get around this difficulty, two approaches have been tried. The first uses the notion of the conspiracy of Regge trajectories, while the second employs absorptive corrections or cuts.

A simple discussion of conspiracy and its application to the np reaction is given by Phillips.[15] The basic idea is that one supposes that there is another trajectory associated with particles of positive parity which has the same value of its trajectory function $\alpha(u)$ at

$u = 0$ as does the pion. This trajectory would contribute to the amplitudes in the same way that the A_2 does, however at $u = 0$ its contribution would have the same phase as that of the pion as well as the same energy dependence. If we call this particle π_c we may then write

$$\phi_3 = \phi_3^{\pi} + \phi_3^{\pi_c} = 0 \quad \text{at} \quad u = 0.$$

This formula does not require $\phi_3^{\pi} = -\phi_2^{\pi}$ to vanish at $u = 0$, but only requires that there be a relation between the residues associated with the π and π_c trajectories. Such a relation is called a conspiracy relation. I should note here that the residue functions are the free functions in the Regge Theory. They are arbitrary except for constraints imposed by physical principles such as angular-momentum conservation and unitarity. If an amplitude must vanish, or assume some particular value at a certain momentum transfer then one arranges the residue to accommodate the constraint.

Since $\phi_2^{\pi_c} \neq -\phi_3^{\pi_c}$, ϕ_2^{π} is now not required to vanish at $u = 0$. There is a non-vanishing contribution of the pion to the cross section at $u = 0$ and the contribution is such that a peak results. Phillips model using ρ, A_2, π, and π_c gives a rough fit to the data. Better fits were obtained by the usual method of using enough trajectories to have the freedom needed given the amount of data available.[16]

There are, however, several problems with using conspiracy. First, no particles have been found which can be associated with the π_c trajectory. Second, the constraint equation which keeps the residue function in ϕ_3^{π} from vanishing restricts the form which this residue can take. This

restriction along with the assumption of factorizability of Regge pole residues lead LeBellac[17] to predict a dip in the forward direction of the cross-section for the reaction $\pi N \to \rho\Delta$. A subsequent experiment[18] which analyzed the reaction $\pi^+ p \to \rho^0 \Delta^{++}$ revealed instead a peak in the forward direction.

The next step in theoretical complexity involves the introduction of Regge cuts. A Regge cut may be generated by a diagram like Fig. 2 in which two Regge poles are exchanged. Most people who use cuts in

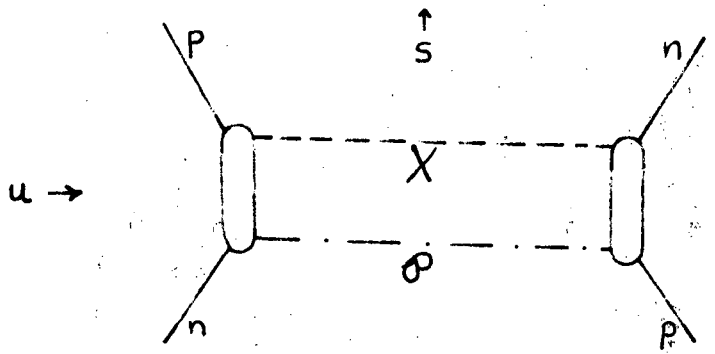

Fig. 2. Two Particle Exchange Diagram for np → pn.

their fits calculate them using a model in which the cut is generated by a process in which the single-pole exchange is accompanied by single- or multiple-elastic scattering.[19] (In Regge language this corresponds to single or multiple Pomeron exchange). The amplitudes generated interfere destructively with the single-Regge exchange amplitude. The peak in the np reaction is then due to the fact that the pion term vanishes while the cut contribution is finite and nonzero at u = 0. The use of cuts seems to

help to fit the data, but by using a formulation which has not yet been well anchored to the Regge framework.

The insight which emerges out of this whole business is meagre indeed. The basic features are clear though:

1) The pion contribution determines the rapid behavior of the cross section near $u = 0$.

2) There is some mechanism possibly conspiracy or absorptive interference which leads to a peak rather than a dip at $u = 0$.

We should also note here that the pion pole cannot contribute to the expression for I_0P since $\phi_3^\pi = -\phi_2^\pi$. This means that any interpretation of the results of this experiment will put constraints on the mechanism involved in the suppression of the π contribution to $d\sigma/du$, not on the pion contribution itself.

III. EXPERIMENTAL DETAILS

A. Beam

The neutron beam was produced at 0° from a copper target located at the final focus of channel I of the external proton beam (EPB) at the Bevatron. The production target was 7.6 cm long, 0.5 cm wide and 0.2 cm high. We chose a production angle of zero degrees in order to get maximum neutron flux and to assure ourselves of a neutron beam which was unpolarized. The particles produced in the target then passed through a bending magnet which was used to direct the proton beam away from 0°. This magnet deflected most of the charged particles so that they did not enter our collimator.

The collimator system is shown in Fig. 3. Before the beam entered the collimator it passed through 2.5 cm (5 radiation lengths) of lead so that any photons in the beam would be converted. The two sections of the collimator were made by taking two pieces of 15.2 cm × 4.9 cm steel channel and welding them together to form a rectangular tube. Steel pipe of various diameters was supported in the center of these tubes and molten lead was poured around the pipe to complete the collimator. The first section of the collimator contained tubes of 5.7 cm diameter, 3.8 cm diameter, and 2.5 cm diameter with the diameter decreasing in the direction of the beam. This stepped design was used in order to minimize the amount of collimator wall near the start of the collimator which could be seen at our polarized proton target. We thus hoped to minimize the halo in the beam associated with scattering from the walls of the collimator. This first section was 80 cm long. The second section was 121 cm long and had a diameter of 1.6 cm. The end of this collimator was

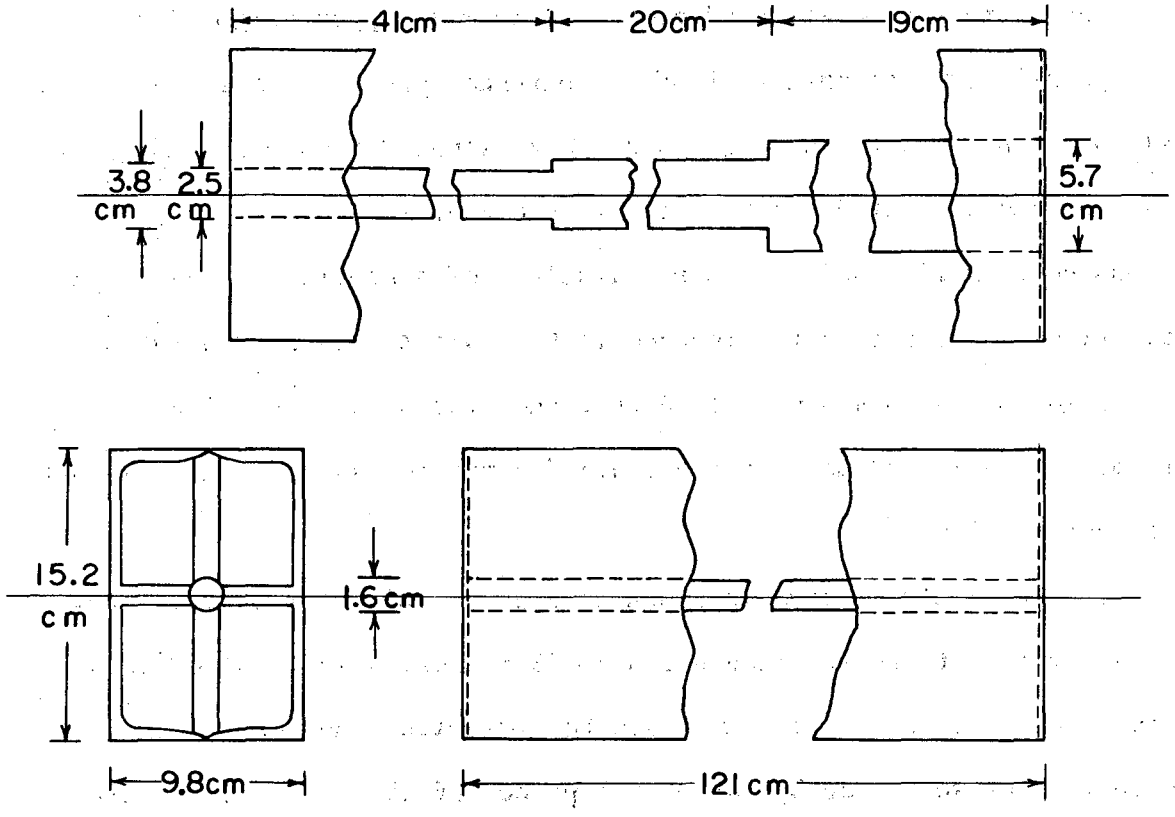

Fig. 3. Neutron Beam Collimators.

located at 4.6 m from the production target giving us a solid angle acceptance of 9.5×10^{-6} steradians. This collimator gave a beam spot of about 3 cm in diameter at our target which was located 8.5 m from the production target. Each section of the collimator had illuminated cross hairs located at each of its ends so that we could align the sections. The illuminated cross-hairs also allowed us to check the collimator alignment after all sections were in place and the shielding wall built.

After the beam passed through the defining collimator, it went through a final sweeping magnet and then through a hole 4.8 cm in diameter in the return yoke of the polarized target magnet. This final collimator was of sufficient diameter so as not to interfere with the main beam. This system gave a beam of about 3×10^6 neutrons for 10^{11} protons incident on the production target. Charged particle contamination of the beam was about .02%, while the gamma ray contamination was 3%. The beam was monitored by two separate 3 counter telescopes located in the beam at the back of our experimental cave where the beam was dumped into a concrete wall.

Fig. 4 shows a momentum spectrum of the beam. This spectrum was obtained by calculating the momentum of the incoming neutron for events which satisfied the kinematic constraints for elastic scattering and had $.03 \leq |u| \leq .2$. We then corrected the number of neutrons in each momentum bin for the solid angle acceptance of our apparatus for events at that momentum. Since the cross-section varies approximately as P_{Lab}^{-2} (where P_{Lab} is the momentum of the incident neutron) independent of momentum transfer, at least for $|u| < .5$, we then scaled the corrected spectrum by P_{Lab}^{2} to get the results in the figure. We used only a

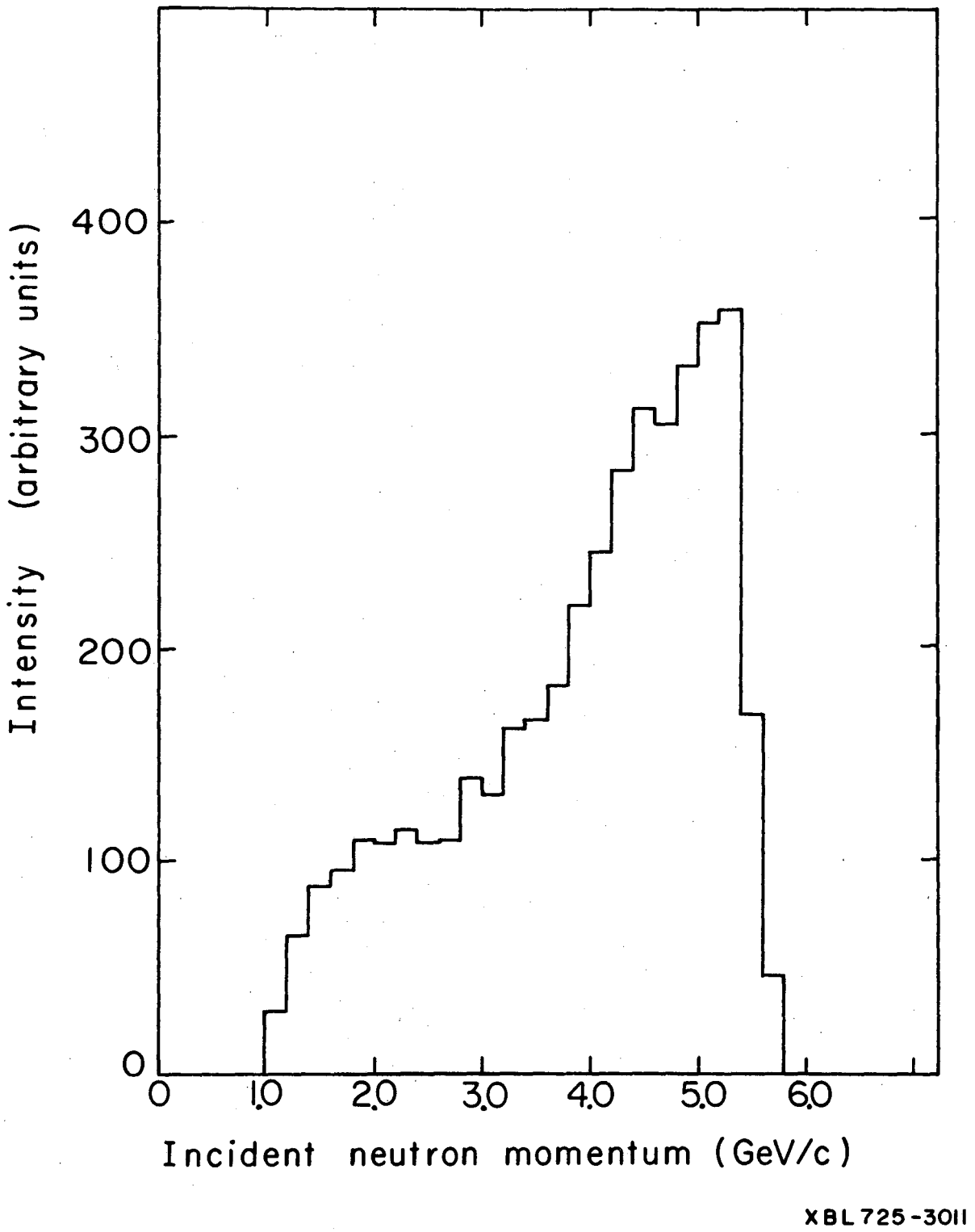

Fig. 4. Neutron Beam Momentum Spectrum.

restricted momentum transfer region to avoid small |u| where our peak/ background ratio was small and large |u| where our momentum transfer acceptance was very momentum dependent.

B. The Polarized Proton Target

The theory and practice of the operation of a polarized proton target have been extensively described elsewhere;[20] A brief qualitative summary will, therefore, suffice. The target we used consisted of about 6 g/cm^2 of $LaMg_3(NO_3)_{12} \cdot 24\ H_2O$ otherwise known as LMN. The protons in the water of hydration were polarized by dynamic nuclear orientation. In this method one puts the sample in a high magnetic field (18 kg) at low temperature (1.0 K) and then uses microwaves of about 70 GHz to saturate double-spin-flip transitions involving the nuclear spins of the protons and the spin of a nearby paramagnetic center (in this case one caused by a Nd^{++} impurity in the LMN crystal lattice). The saturation of these double-spin-flip transitions coupled with a slow proton relaxation time and a fast relaxation time for the paramagnetic spins leads to a substantial net polarization of the protons. In this experiment the protons, which were about 3% of the target by weight, had a typical polarization of 50%.

The polarization is determined by measuring the amount of energy absorbed or emitted by the sample when some of the protons make spin-flip transitions under the influence of a small applied RF field (i.e. by standard NMR techniques). When the protons are aligned with the field (defined as positive polarization) they are in their lowest energy state and therefore absorb energy from the applied RF field in making transitions; when they are anti-aligned they emit energy. The LMN sample is placed in a coil which is the inductor of a tuned circuit. The target, by absorbing or emitting RF energy inside this coil, acts like a positive or negative resistance and therefore modifies

the impedance of the coil. Using a constant current RF source we detect the voltage across the tuned circuit, and therefore measure its impedance. This impedance measurement is then used to determine the polarization of the sample. The whole system is calibrated by measuring the thermal equilibrium signal from the sample at a known temperature in the absence of microwave radiation. Knowledge of the temperature and the magnetic field allows one to calculate the polarization at thermal equilibrium, since the two orientations of spin are populated according to the Boltzman factor.

Figure 5[23] shows a block diagram of the NMR detection apparatus. Details of this apparatus are available elsewhere.[21] The operation of the system is controlled by a PDP-5 computer (in this experiment the computer was also used to monitor other aspects of the experiment). The computer sets the RF frequencies used to sweep out the NMR signal and a range of background on either side of the signal. As the RF frequency is swept through the signal, the capacitor in the tuned circuit is also varied so that the circuit is always tuned to a resonant frequency corresponding to the RF oscillator frequency. The circuit is kept at resonance, since then the impedance has a particularly simple form, namely $|Z| = (\omega L)^2 / R$ (neglecting a term of order $1/|Z|$). The output voltage across the tuned circuit is then amplified and converted to a D.C. level with a diode. This D.C. level is transmitted to the computer by means of a Voltage-to-Frequency converter (V.F.C.) A circuit controlled by the computer converts this frequency to a number by using 100 of these V.F.C. pulses (the frequencies were $\sim$100 Kc) to determine

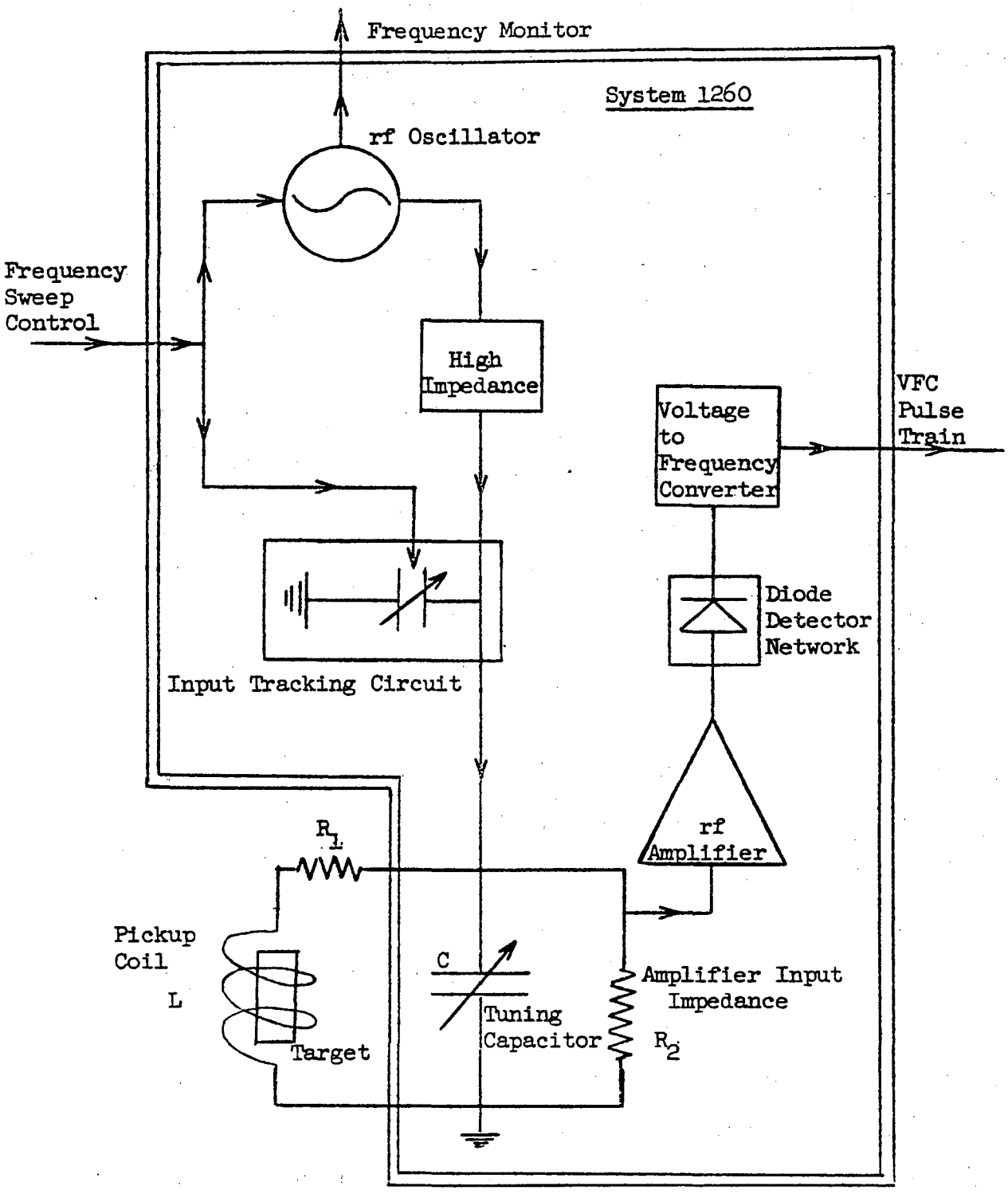

Fig. 5. Polarized Target NMR Detection Apparatus.

the time during which a 100 Mc oscillator is allowed to feed pulses into a scaler. The number in the scaler after it has been gated on and off by the pulses from the VFC is proportional to the inverse of the RF voltage. We use the inverse of the voltage since it is directly proportional to the resistive component of the impedance.

This computer-controlled readout is able to complete a sweep through the signal in roughly 2 seconds, so that we were able to monitor the polarization after every Bevatron pulse. The entire signal was dumped onto magnetic tape after every readout. We reversed the sign of the polarization typically every 90 minutes in order to minimize the effects of long term drifts of our apparatus. The computer also made a display which showed the line shape of the signal we were looking at. Figure 6 shows examples of this display for negative polarization and the thermal equilibrium signal.

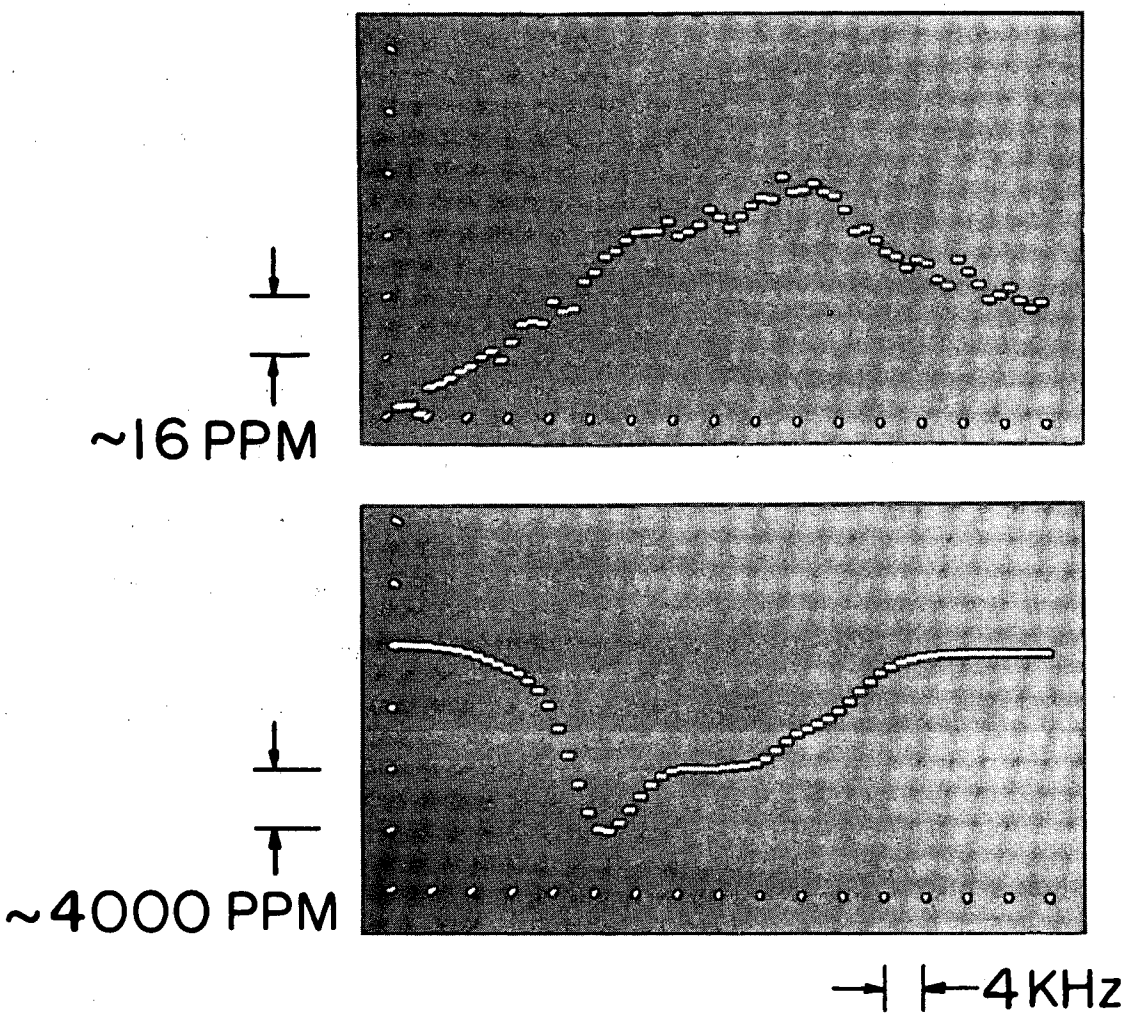

Fig. 6. Computer Display of NMR Signals.

C. Detectors

The basic problem in the design of a detector system was to identify an event in which an incident neutron of unknown momentum elastically scattered from a proton in our target sending the proton forward with large momentum. The neutron, at the same time, would have been scattered near 90° from the beam direction. We wished to measure the scattering angles and the momentum of the forward proton and also the scattering angle and energy of the neutron in order to have enough information to pick out elastic scattering events clearly, and to distinguish them from the quasi-elastic scattering of neutrons from protons in heavy nuclei in our target. At the same time, we wished to determine the momentum of the incident neutron. In order to do this we set up a system consisting of a set of counters which produced a trigger when there was an event candidate, a magnetic spectrometer which was used to measure the scattering angle and momentum of an outgoing, forward, charged particle and an array of neutron counters located below the target. A schematic of this system is shown in Fig. 7.

C1 -- Trigger

Our trigger required that a neutral particle strike the target, that a charged particle go forward through the spectrometer, and that a neutral particle interact in our neutron detectors. To assure that only incident neutral particles would be considered we placed a 3 mm thick scintillation counter 62 cm upstream of the target and used it in anti-coincidence. The forward charged particle was required to pass through

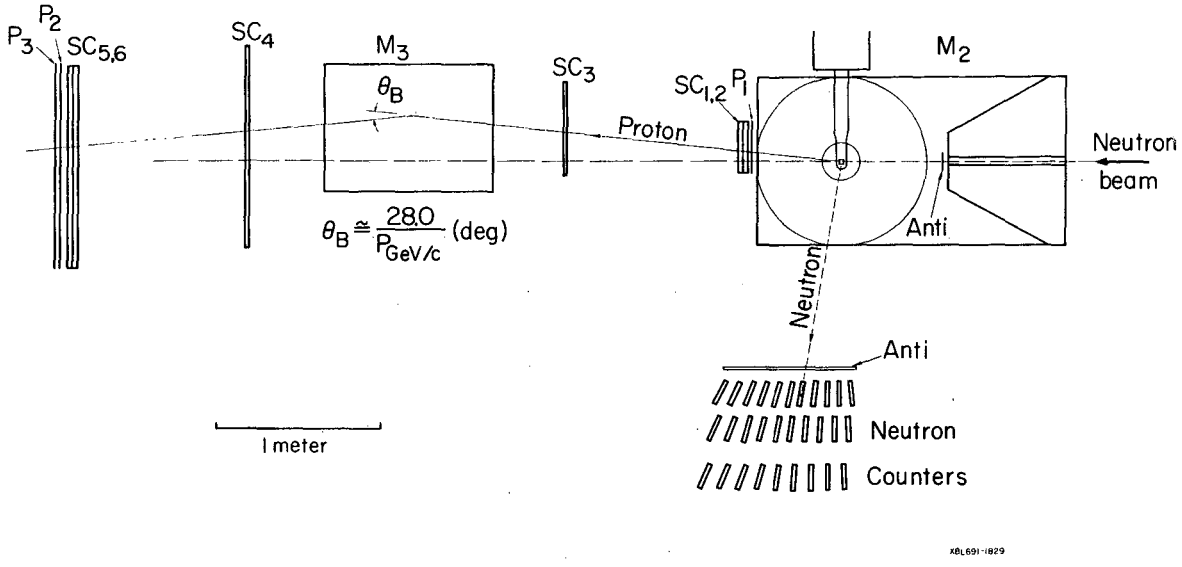

Fig. 7. Side View of the Experimental Detector System.

three counters, P1, P2, P3. P1 was located 60 cm downstream of the target and before the first spark chamber. P2 and P3 were located 470 cm downstream of the target, after the spectrometer magnet and directly downstream of the last spark chamber. P1 was 3 mm thick to minimize the effect of multiple scattering on the determination of the proton scattering angles.

We required that particles detected in our neutron counters not be detected in a layer of anti-counters placed directly over the neutron counters. We placed anti-counters over the accessible regions of the polarized target magnet poles and also placed anti-counters so as to intercept charged particles going down and forward or up and forward which could not count in P1. (These antis are not shown in Fig. 7). The most useful antis were those on the magnet poles downstream of the target and those over the neutron counters. A schematic of the circuit used to transform the information from these counters into a trigger is shown in Fig. 8. The trigger formed was then used to initiate the firing of the wire chambers and to inform the on-line computer that an event had occurred.

The schematic of Fig. 8a also shows the main component of the trigger which was the coincidence between the output of the logic element PAND (which required that a neutral come in and a charged particle go forward) and the signals from the neutron array. This coincidence occurred in the Fast Logic Boxes which will be described later when we discuss the neutron detectors. One of the troubles with this whole setup was that

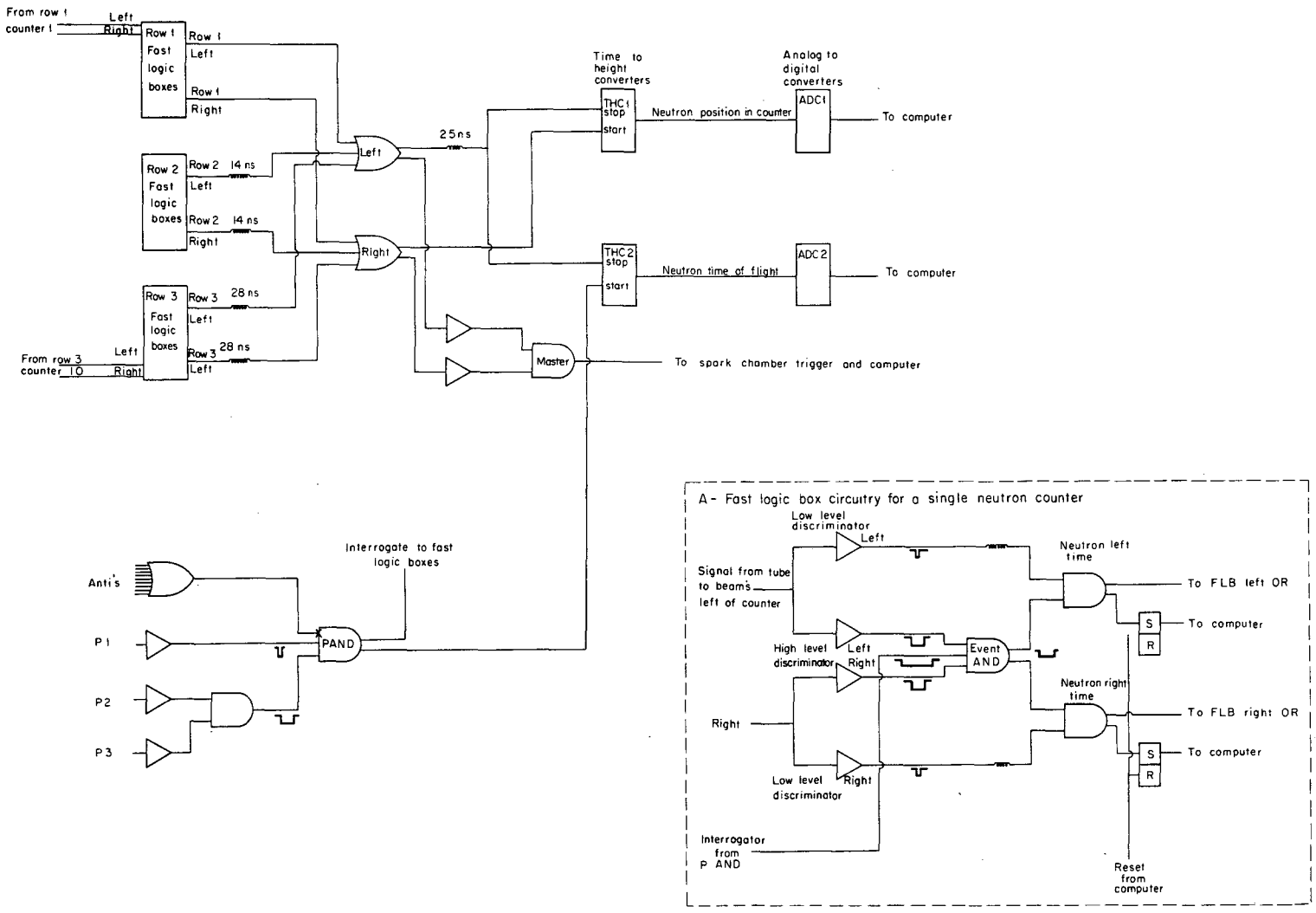

Fig. 8. Event Trigger Logic and Logic Schematic for a Single Neutron Counter in a Fast Logic Box.

XBL725-3001

the PAND signal had to wait for the slowest possible elastically scattered neutron (about 80 ns), thereby delaying the trigger and the firing of the spark chambers. We were also hurt by the fact that our electronics was constrained by space limitations to be set up rather far from the apparatus. This combination of circumstances meant a delay of about 450 ns between an event and the firing of our chambers. This led to a low efficiency for the spark chamber system. While for most of the chambers the individual gap efficiencies appeared to be well over 95%, our track recovery of about 40% means that each chamber was only about 80% efficient for the particles in which we were interested. The remainder of the sparks we recorded were spurious--they were not due to accidentals in the PAND coincidence since we kept accidentals in this coincidence below 5%.

C2 -- Spark Chambers and Spectrometer

The spark chambers were wire chambers each having a gap of 9 mm and a wire spacing of 1 mm. Six chambers were used in the experiment, three before and three after the spectrometer bending magnet, as shown in Fig. 7. The first chamber (SC1), which had wires parallel and perpendicular to the vertical (90° chamber), was located 62 cm downstream of the production target and had an active area of 14.6×25.4 cm^2. The second chamber (SC2) with wires at 45° with the vertical (45° chamber) was located 6.1 cm downstream of SC1 and had the same active area. The third chamber (SC3) a 90° chamber, was located 100 cm downstream of SC1 and had an active area of 22.8×50.8 cm^2. This chamber was located 94 cm upstream of the

center of the bending magnet. The chambers in back of the magnet all had active areas of 38.1 × 114 cm^2. The fourth chamber (SC4), a 90° chamber, was located 94 cm downstream of the center of the bending magnet. The fifth chamber (SC5), a 45° chamber, was located 93.9 cm downstream of SC4 while the final chamber (SC6), a 90° chamber, was located 100 cm downstream of SC4. The 45° chambers were used to untangle the ambiguity caused when two tracks went through the closest 90° chamber.

The spectrometer magnet was run at 16.1 Kg to give a bending angle of about [28 GeV/c / momentum(GeV/c)] degrees and bent protons down. Since the protons in which we were interested would scatter up from the target, this mode of operation allowed us to get a larger solid angle acceptance than if we had bent the scattered particles up. The neutron beam ran right through the chambers. This did not seem to cause us much trouble, though it may have added to the problems we already had because of the slow spark chamber trigger. The position of a spark in a chamber was recorded by means of a magnetostrictive readout which digitized the location in two perpendicular directions. This information was transferred to our on-line computer and eventually logged on magnetic tape. The readout was capable of handling only two simultaneous sparks in a chamber.

The spark chamber gas was the usual neon-helium mixture. We passed about 5% of the gas through a pot of ethyl alcohol vapor in order to cut down spurious sparking. This also seemed to help edge sparking

problems. The chambers were usually run at 8.5 Kv with a clearing field of about 50 v. We usually pulsed the chambers at rates of 20-30 triggers per second and in order to do this had to blow air through our spark gaps to prevent their breakdown when they were rapidly recharged. We also gated the circuitry so that after an event we waited ∿25 msec before gating the trigger circuit on again.

C3 - Neutron Counters

Recoil neutrons from the target were detected in an array of scintillation counters located below the target. There were 30 counters in the array and they covered neutron laboratory angles of from 91° to 61°, with each counter having an acceptance angle of about 1°. The counters were 2.5 x 15 x 96 cm^3 where the long axis was perpendicular to the plane of Fig. 7. A detail of one of these counters is shown in Fig. 9. An RCA 8575 phototube was located at each end of the scintillator. We determined the position along the long axis of the counter in which a neutron interacted by measuring the time difference between the arrival of the scintillation light at each of the two phototubes. One cannot do a very good job of measuring this time difference by simply measuring the time difference between the outputs of two discriminators triggered by the phototube pulses, since the time at which the discriminator fires is determined by the amplitude of the phototube pulse. This phenomenon is usually called "time slewing". Since neutrons interacting in the scintillator yield charged particles which deposit widely varying amounts of energy in the scintillator, this problem would have been severe. In order to combat it we designed a system which required that

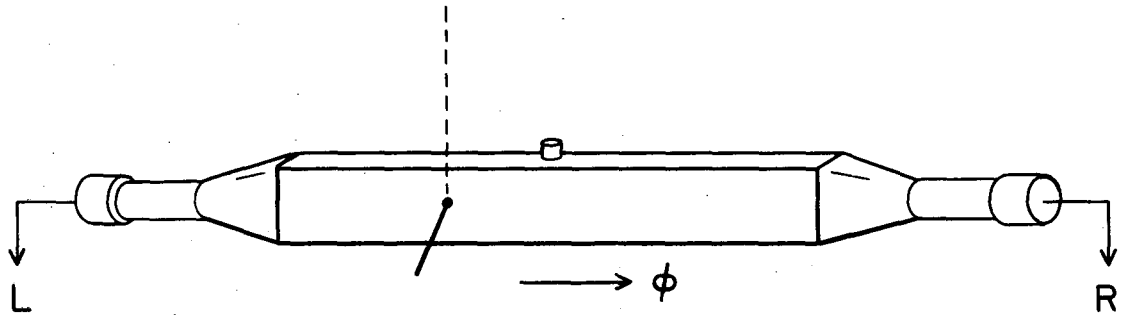

$$\phi = t_L - t_R$$

$$T.O.F. = 1/2\ (t_L + t_R)$$

XBL691-1735

Fig. 9. Detail of a Neutron Counter.

the pulses from the tubes have a certain minimum amplitude and then triggered our timing discriminators on these same pulses but at 1/2 the minimum amplitude.

The circuit which we used to do this job is shown in Fig. 8a. The signal from each of the tubes was split using a transformer. One of the resulting signals then triggered a discriminator set at 1 v , while the other triggered one set at 2 v. The outputs of the high level discriminators for Left and Right were then required to form a coincidence with each other and with a signal from the fast trigger indicating that a charged particle had passed through the spectrometer. This was our master coincidence. The output of this circuit then opened a gate which allowed the pulse from the low level discriminator to pass. This pulse then went on to the timing circuitry while another pulse from the same gate set a flip-flop which indicated to the computer which counter had fired. One of these circuits was required for each counter and they were put together in bins which serviced five counters (these were the Fast-Logic Boxes referred to earlier).

Figure 7 shows the counters arranged in three rows. This was done to minimize the ambiguity caused when a recoil charged particle from a neutron interaction enters an adjacent counter. If counters N and N + 1 fire, then if they are not staggered we do not know in which of them the neutron initially interacted. However, if they are, then the counter in the row closest to the target is the source of the interaction. Of course, if counters N and N + 3 fire then we are confused, and so we ignore events of that type (about 7% of the events were ambiguous in this way). We arranged the timing circuitry so that when several counters fired, the pulses from the counter nearest the target were recorded.

The timing circuitry consisted of a time-to-height converter (THC) and an analog-to-digital converter (ADC). The signals from the right side of the array always arrived at the THC first and initiated its operation. The signals from the left side then provided the stop signal. Signals from the left side were also used along with a signal from the PAND coincidence to measure the time difference between the firing of counter P1 and the neutron counter associated with that event (the firing of PAND was of course determined by the time of arrival of the P1 signal at PAND). This time measurement allowed us to determine the time of flight of the neutron.

In order to provide a monitor of the operation of the neutron counters during the experiment and correct for any drifts in the system, we placed light pulsers on the scintillators half-way between the two tubes. Every few hours we pulsed each of the pulsers 120 times to determine the ADC number which corresponded to the center of the counter in order to calibrate our position measurement. The computer made plots of the distribution of positions from a pulser run so that we could see if any of the circuitry was not performing up to our expectations.

In actual operation we were able to find the position of the neutron along the long axis of one of these counters with an uncertainty of about 8 cm (FWHM). This uncertainty corresponds to a relative time of flight resolution of 1.2 ns (FWHM). Figure 10 shows a distribution of the deviations of expected position from measured position for one of our counters. This shows the virtue of using this type of system. In order to get this resolution

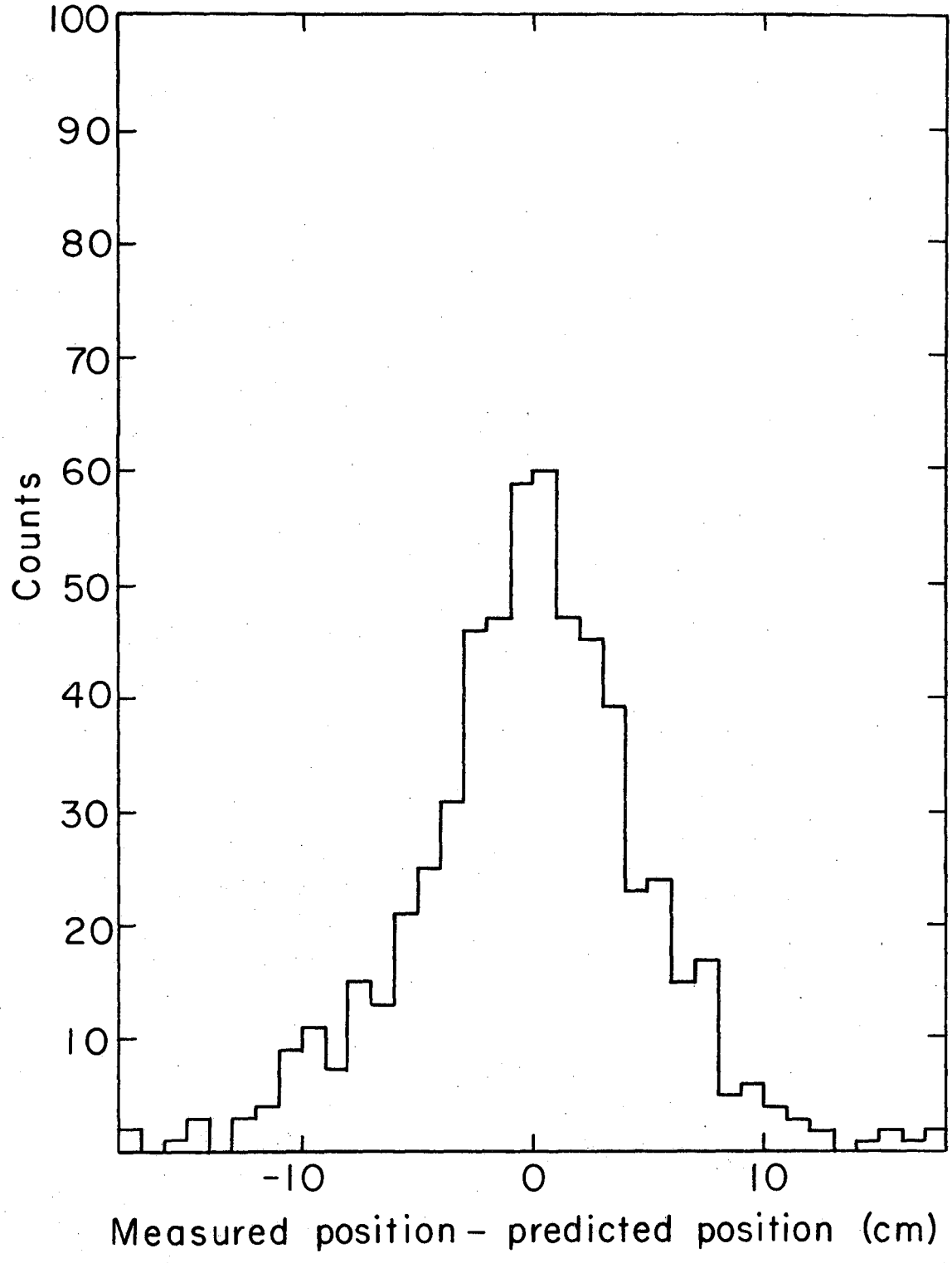

XBL725-3010

Fig. 10. Deviation of Expected Position from Measured Position for a Neutron Counter.

using single counters, each with its own phototube, one would need at least ten times as many of them. One might think that the added circuitry makes up for this cost, but the timing discriminators were very simple tunnel-diode discriminators which were already available and the high level discriminator and master coincidence circuit were made using integrated circuits. Our absolute time of flight resolution ranged from about ±8 ns for neutrons emerging near 90° to ±1.5 ns for neutrons with angles near 60°.

In order to do relative timing in this way, however, we had to make the coincidence between the signal from the forward proton and that from each neutron counter rather broad. For neutrons at angles of 63° to 76°, the width of the proton signal was 33 ns, while for neutrons with angles greater than 76° the width was 47 ns in order to account for the spread in neutron time-of-flight to a single counter. These large widths coupled with a neutron singles rate of about 7.5×10^5 neutrons for 2×10^{11} protons on the production target led to an accidental coincidence rate of 15-20%. In order to get to this tolerable rate we had to do extensive shielding of the experimental area, since a main source of counts in the neutron array was slow neutrons coming from all directions through the shielding around our experiment. In fact, even after our shielding efforts, the counting rate in the array dropped by only a factor of two when we lowered a beam plug into our collimator.

C4: Data Acquisition and Monitoring:

The data from all of these detecting devices were eventually read and stored by a PDP-5 computer. The computer collected data during one Bevatron pulse and then, between pulses, wrote the accumulated data on magnetic tape. It also controlled the polarization readout electronics, stored the data accumulated during a measurement of the target NMR signal and wrote these data on tape. The computer was programmed to calculate the target polarization and display the NMR signal on an oscilloscope so that we could monitor the polarization and try to maximize it. The program also did some on-line analysis of the data. Using the spark-chamber information it reconstructed outgoing particle trajectories in the horizontal and vertical planes (non-bending and bending planes) and displayed these trajectories. It reconstructed the apparent point of origin of the trajectory and displayed a distribution of points of origin so that we were able to "see" our target and check that the beam was not scattering from anything else. The computer also plotted distributions of the number of sparks as a function of their position for each chamber so that we could check to see if the chambers were breaking down preferentially anywhere. The computer used the neutron counter data to make up a plot of the distribution of counts in the neutron array so that we could determine if a counter was malfunctioning. We also checked the counters by using the light pulsers to pulse each counter sequentially. The program controlled this sequencing, provided displays to check the operation of the counters when pulsed, and stored the pulser data on tape for later use.

IV. ANALYSIS

A. Picking Out Elastic Events

The data tapes contained for each event the co-ordinates of the sparks in our chambers, the identity of the neutron counter which fired, the time of flight of that neutron, and its position along a line perpendicular to the vertical plane of the experiment. The analysis commenced by finding the scattering angles θ_p, ϕ_p of the proton, its momentum, the scattering angles θ_n, ϕ_n of the recoil neutron and its time of flight. The positions of the spark chambers were determined by a survey, but in order to further refine our knowledge of their relative positions we took data with the spectrometer bending magnet turned off. This gave us a series of "straight through" events. We then made a fit to the hypothesis of a straight line for each of these events and using this fit made small corrections to our measurements of the positions of our chambers in order to get good fits. In this way we were able to correct for any accidental small disturbance of the chamber positions.

In order for an event to be considered in the analysis we required that there be a straight line fit to its trajectory before and after the magnet, that these trajectories intersect inside the magnet, that the trajectory before the magnet appear to come from our target, and that neither trajectory appear to hit the spectrometer magnet. We tried to recover some events in which we had only one straight line, either before or after the magnet, and one point which seemed to lie on the same trajectory, but the quality of the fits obtained was significantly lower, so that we decided to ignore such events. The field of the spectrometer had been mapped before the experiment and it was uniform enough

to justify using an effective length, constant field approximation so that we did not have to integrate each orbit through the field to find its momentum. We merely calculated the angle between the trajectory before the magnet and that after it and obtained the momentum directly. Using the trajectory before the magnet we could calculate the angles θ_p, ϕ_p making a small correction to θ_p to account for bending in the polarized target magnet.

The neutron angles θ_n, ϕ_n were determined by knowing which neutron counter fired and determining the position of the neutron interaction along the long axis of that counter by using the relative time of flight information. The absolute time of flight (TOF) of the neutron was measured directly. If an event had a good charged particle track and there was no ambiguity in the identity of the counter in which the recoil neutron interacted, we accepted it as a "good" event and proceeded with the analysis.

In the next stage of the analysis we used the kinematical quantities for each event to determine whether it was elastic scattering. We used θ_p, ϕ_p and the momentum of the outgoing proton to calculate the kinematical quantities $\tilde{\theta}_N$, $\tilde{\phi}_N$, $\widetilde{TOF}$, that one would expect for the neutron if the event had been elastic np scattering. We then made up a distribution of the number of events versus the quantities $\theta_N - \tilde{\theta}_N$, $\phi_N - \tilde{\phi}_N$ and TOF - $\widetilde{TOF}$. If a scatter plot is made in which each of these quantities was marked off on the axis of a 3 dimensional plot there is a cluster of events at the origin corresponding to elastic scattering. For a typical momentum transfer this clustering has a width of ±5 ns in TOF and a width in ϕ which depends on the momentum transfer. Fig. 11 shows a typical

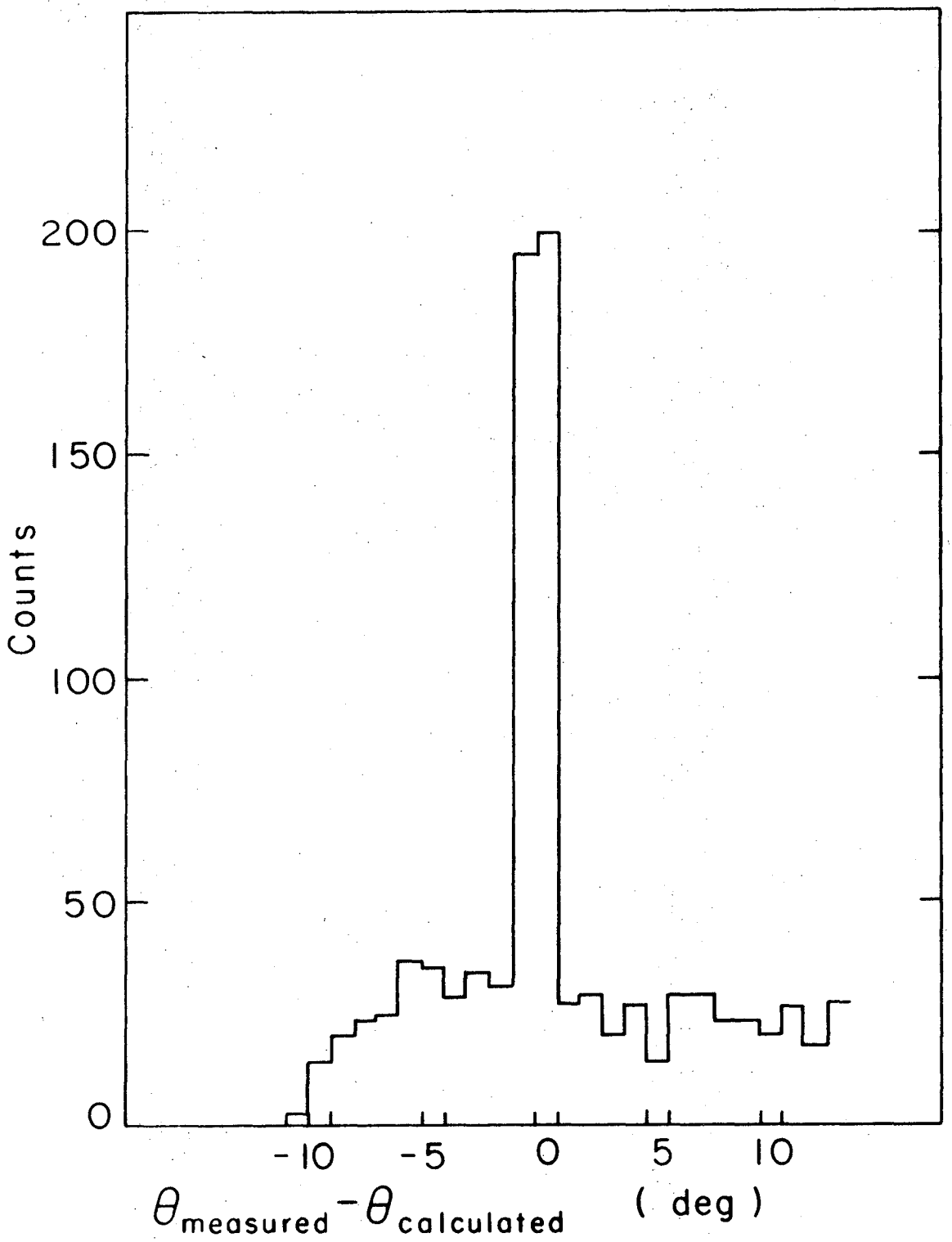

Fig. 11. Deviation of Scattered Neutron Angle from Angle Calculated Assuming Elastic Scattering.

distribution in θ for those events which fall near the origin in the ϕ and TOF distributions. This plot shows a clear peak at the origin which corresponds to elastic np scattering with a peak to background ratio of about 6.

In order to determine the background under the peak so that we can find the number of neutrons elastically scattered from free protons, we considered a two dimensional plot like that in Fig. 12 for which events have TOF's corresponding to elastic scattering. There are four regions in this distribution labeled P, N, B, M. P contained those events consistent in all variables with elastic scattering, N those events consistent in θ but clearly not consistent in ϕ, B those events consistent in ϕ but clearly not in θ, and M those events clearly inconsistent in both θ and ϕ. We assumed that those events for which ϕ is inconsistent with elastic scattering represent the inelastic and quasi-elastic background. We then took the ratio of the number of counts in region B to that in region M and multiplied the number of counts in region N by the result to get the background in region P. In other words we used the tails of the θ distribution for the coplanar and non-coplanar events to determine the normalization of the non-coplanar events which had θ's consistent with the hypothesis of elastic scattering (the background under the elastic peak). We checked this background determination by taking data with a dummy target similar in composition to the polarized target, but which contained no free dydrogen. Fig. 13 shows a typical θ distribution of coplanar events taken from the dummy data compared with a θ distribution of non-coplanar events taken from target data. Clearly, the two methods of background determination are consistent.

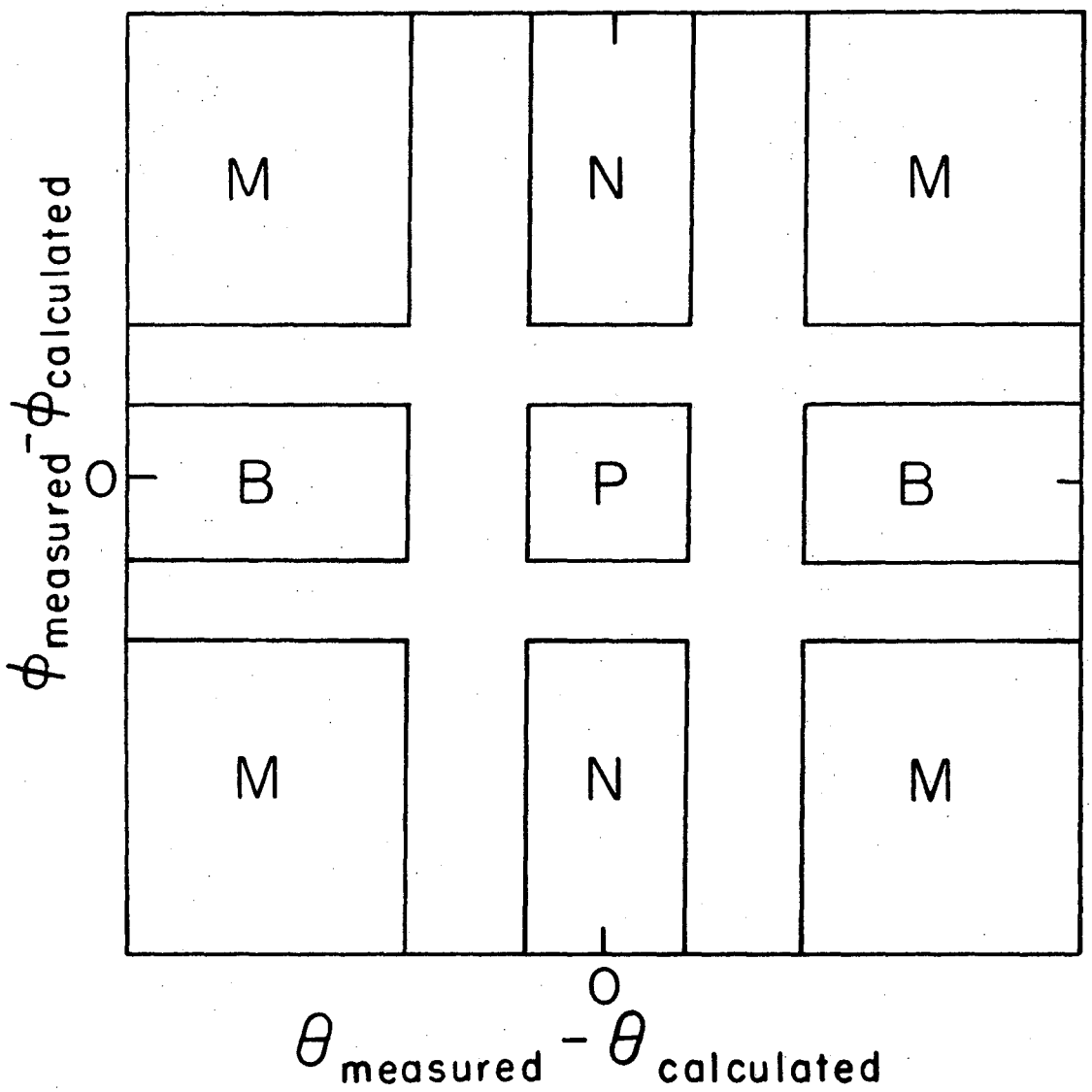

XBL725 - 3008

Fig. 12. Diagram Showing Regions in θ and ϕ Used for Determination of the Background Under the Elastic Scattering Peak.

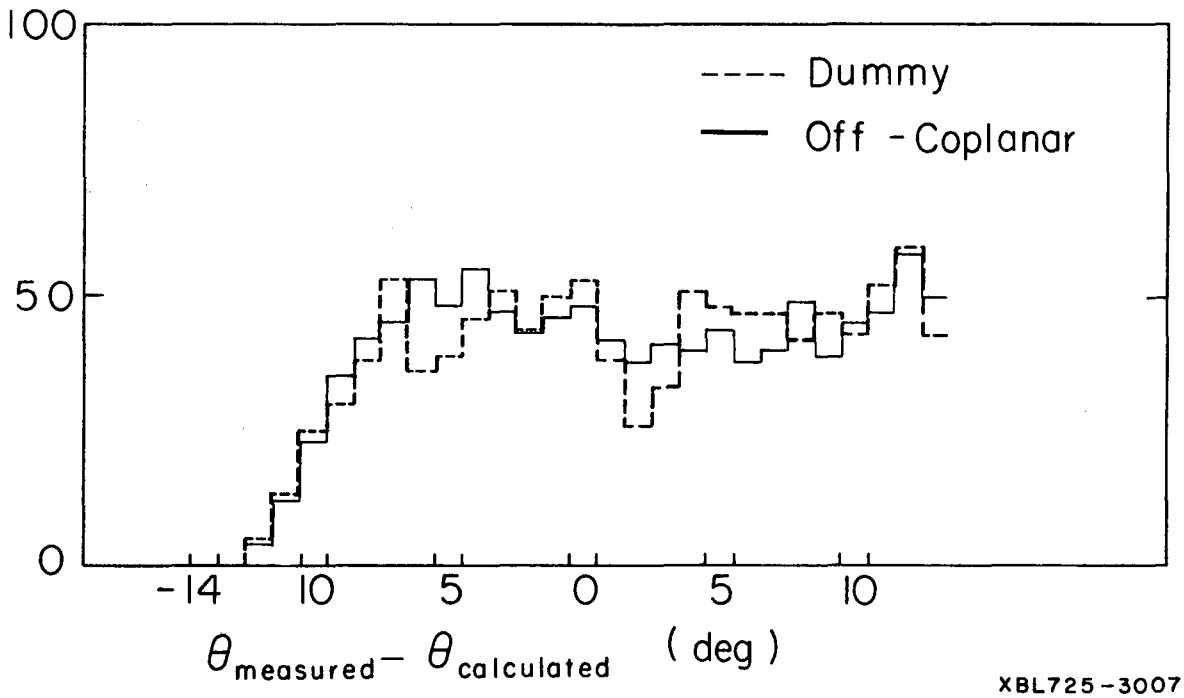

Fig. 13. Comparison of Coplanar Dummy Data with Off-Coplanar Polarized Target Data.

B. Calculation of the Asymmetry

We have a set of measurements of N_i, M_i, and P_i. These are respectively the number of elastic events in the i^{th} run, the number of monitor counts in the i^{th} run and the polarization of the target during the i^{th} run. We wish to find a value for A so that the function $f(I_0,A) = M_i I_0(1 + A\ P_i)$ best represents N_i. In order to do this we perform a least squares fit, in which we minimize the quantity:

$$S = \sum_i \frac{[N_i - M_i(I_0 + I_0\ A\ P_i)]^2}{\sigma_i^2}$$

where σ_i^2 is the mean square error of the i^{th} measurement of N_i. If N_i were large, we would assume that its mean square error were equal to N_i (that is, we would assume a Gaussian distribution). In our case N_i is usually small enough so that we must consider using Poisson statistics. For a Poisson distribution, σ_i^2 is just the expected value of N_i. However we do not know the expected value of N_i until we have solved the problem. At that point we would have parameters $\bar{A}$, $\bar{I}_0$ and find $\sigma_i^2 = M_i(\bar{I}_0 + \bar{I}_0\ \bar{A}\ P_i)$. It is important to realize that σ_i^2 is not a function of I_0,A, but only of the final values $\bar{I}_0$,$\bar{A}$. That is σ_i^2 is the error in the measurement, it cannot depend on what function we use to describe the measurement. A priori, we do not know σ_i^2, but after the fact we can estimate it by using the function we have found. Since σ_i^2 is characteristic of the accuracy of the measurement of N_i, we treat it as a measurement, not a parameter, when we minimize S. In order to find the minimum of S we solve the set of equations:

$$\frac{\partial S}{\partial I_0} = 0 \qquad \frac{\partial S}{\partial I_1} = 0$$

where $A \equiv I_1/I_0$

$$\frac{\partial S}{\partial I_0} = 0 = \sum_i \frac{M_i}{\sigma_i^2}\left[N_i - M_i(I_0 + I_1 P_i)\right] \tag{1}$$

$$\frac{\partial S}{\partial I_1} = 0 = \sum_i \frac{M_i P_i}{\sigma_i^2}\left[N_i - M_i(I_0 + I_1 P_i)\right] \tag{2}$$

Solving for I_0 we get

$$I_0 = \frac{\sum_i \frac{M_i N_i}{\sigma_i^2}}{\sum_i \frac{M_i^2}{\sigma_1^2}(1 + A P_i)} \qquad \text{from (1)}$$

$$I_0 = \frac{\sum_i \frac{M_i N_i P_i}{\sigma_i^2}}{\sum_i \frac{M_i^2 P_i (1 + A P_i)}{\sigma_i^2}} \qquad \text{from (2)}$$

Now setting them equal:

$$\sum_i \frac{M_i N_i P_i}{\sigma_i^2} \sum_j \frac{M_j^2 (1 + A P_j)}{\sigma_j^2} = \sum_i \frac{M_i N_i}{\sigma_i^2} \sum_j \frac{M_j^2 P_j (1 + A P_j)}{\sigma_j^2} \tag{3}$$

After some algebra:

$$A = \frac{\sum_i \frac{M_i N_i P_i}{\sigma_i^2} - \langle p \rangle \sum_i \frac{M_i N_i}{\sigma_i^2}}{\langle p^2 \rangle \sum_i \frac{M_i N_i}{\sigma_i^2} - \langle p \rangle \sum_i \frac{M_i N_i P_i}{\sigma_i^2}} \tag{4}$$

where

$$\langle p^n \rangle \equiv \frac{\sum_j \frac{M_j^2 P_j^n}{\sigma_j^2}}{\sum_j \frac{M_j^2}{\sigma_j^2}} \tag{5}$$

The reason for this definition will be clear in a moment.

Now the question remains what to use for σ_i^2. If we knew the answer $\bar{I}_0 \bar{A}$ then we could use $\sigma_i^2 = M_i \bar{I}_0 (1 + \bar{A} P_i)$ since that would be the expected value of N_i and hence its mean square error. We can determine $\bar{A}$ by a method of successive approximations. First choose $\sigma_i^2 = M_i \bar{I}_0$. That is, since we have no a priori knowledge of $\bar{A}$, assume it to be zero. Then we get a zeroth approximation for $\bar{A}$

$$A^0 = \frac{\sum_i N_i P_i - \langle p \rangle_0 \sum_i N_i}{\langle p^2 \rangle_0 \sum_i N_i - \langle p \rangle_0 \sum N_i P_i} \tag{6}$$

with

$$\langle p^n \rangle_0 = \frac{\sum_i M_i P_i^n}{\sum M_i} \tag{7}$$

In this zeroth approximation $\langle p^n \rangle$ is indeed the n^{th} moment of the target polarization. Now we can use A^0 to set $\sigma_i^2 = (1 + A^0 P_i) I_o M_i$ and find A^1. We can continue to do this until the process converges, that is until $A^{n+1} = A^n = \bar{A}$ (the answer). We note that the zeroth approximation corresponds to the way in which the polarization parameter

has been calculated in many previous measurements.[22] If one does not use successive approximations, one is led from Eq. (3) to the equation:

$$\sum_i \frac{N_i P_i}{(1 + A P_i)} \sum_j M_j = \sum_i \frac{N_i}{(1 + A P_i)} \sum_j M_j P_j$$

or

$$\sum_i \frac{N_i P_i}{(1 + A P_i)} = \langle p \rangle_0 \sum_i \frac{N_i}{(1 + A P_i)} \tag{8}$$

where we have just substituted $\sigma_i^2 = (1 + A P_i) I_o M_i$. This equation is a bit ugly since it is not easy to disentangle A in order to get an answer.

All of this is designed to show the right way to do things, but now we will show that in our case the approximation which yields A^0 is good enough. That approximation corresponds to setting $\epsilon = \delta = 0$ where:

$$\frac{\partial S^0}{\partial I_0} = \frac{1}{I_0} \sum_i N_i - M_i(I_0 + I_1 P_i) \equiv \delta$$

S^0 is the zeroth approximation to S

$$\frac{\partial S^0}{\partial I_1} = \frac{1}{I_0} \sum_i N_i P_i - M_i P_i (I_0 + I_1 P_i) \equiv \epsilon$$

Whereas in reality we have

$$\frac{\partial S}{\partial I_0} = 0 = \sum_i \frac{N_i - M_i(I_0 + I_1 P_i)}{(I_0 + I_1 P_i)}$$

$$\frac{\partial S}{\partial I_1} = 0 = \sum_i \frac{N_i P_i - M_i P_i (I_0 + I_1 P_i)}{(I_0 + I_1 P_i)}$$

Now

$$\delta = \frac{\partial S^0}{\partial I_0} - \frac{\partial S}{\partial I_0} = \sum_i [N_i - M_i(I_0 + I_i P_i)] \left\{ \frac{1}{I_0} - \frac{1}{(I_0 + I_1 P_i)} \right\} \tag{9}$$

$$= \sum [N_i - M_i(I_0 + I_1 P_i)] \frac{I_1 P_i}{(I_0 + I_1 P_i) I_0} = \frac{I_1}{I_0} \frac{\partial S}{\partial I_1} = 0$$

So $\frac{\partial S}{\partial I_0} = 0$ and $\frac{\partial S}{\partial I_1} = 0$ imply $\frac{\partial S^0}{\partial I_0} = 0.$

If we now use

$$\frac{\partial S^0}{\partial I_1} = \varepsilon \quad \text{and} \quad \frac{\partial S^0}{\partial I_0} = 0$$

We get

$$A = \frac{\sum_i N_i P_i - \langle p \rangle_0 \sum_i N_i - \varepsilon \sum_i N_i / \sum_j M_j}{\langle p^2 \rangle_0 \sum_i N_i - \langle p \rangle_0 \sum_i N_i P_i}$$

Or finally:

$$A = A^0 - \frac{\varepsilon \sum_i N_i / \sum_j M_j}{\langle p^2 \rangle_0 \sum_i N_i - \langle p \rangle_0 \sum_i N_i P_i} \tag{10}$$

Now we wish to get an idea of the size of ε . Consider

$$\varepsilon = \frac{\partial S^0}{\partial I_1} = \frac{\partial S^0}{\partial I_1} - \frac{\partial S}{\partial I_1} = \frac{I_1}{I_0} \sum_i \left\{ \frac{N_i P_i^2}{I_0 + I_1 P_i} - M_i P_i^2 \right\}$$

$$= \frac{I_1}{I_0} \left\{ \sum_i^+ \left(\frac{N_i P_i^2}{I_0 + I_1 P_i} - M_i P_i^2 \right) + \sum_i^- \left(\frac{N_i P_i^2}{I_0 + I_1 P_i} - M_i P_i^2 \right) \right\} \tag{11}$$

Where $\sum^{\pm}$ refers to the sum over ± target polarizations. Now in our case P_{i+} and P_{i-} were very nearly constant throughout the experiment so that $P_{i\pm}^2 \cong \langle P_\pm \rangle^2$. Therefore

$$\varepsilon = \frac{I_1}{I_0}\left\{ \langle P_+\rangle^2 \sum_i^+ \left(\frac{N_i}{I_0 + I_1 P_i} - M_i\right) + \langle P_-\rangle^2 \sum^- (....) \right\}$$

Now if we had taken only data with + polarization then

$$\sum_i^+ \left(\frac{N_i}{I_0 + I_1 P_i} - M_i \right) = \frac{\partial S}{\partial I_0}$$

must vanish for the correct value of A, similarly $\sum^-$ must also vanish. If the value of A we determine from using both plus and minus polarization is right, then both sums are small (note that if $\langle p_+\rangle^2 = \langle P_-\rangle^2$, as is nearly true in our case, we get $\varepsilon \cong \frac{I_1}{I_0} \langle P^2\rangle \frac{\partial S}{\partial I_0}$ directly, proving that it is small).

The reason that the zeroth approximation is so good is that we are fitting a straight line

$$N_i = (I_0 + I_1 P_i) M_i$$

to essentially 2 points when $P_i^+ \cong P^+$ and $P_i^- \cong P^-$. If either P_i^+ P_i^- vary considerably during the experiment then one must use the iterative procedure to get the correct answer. We should note also that if A is small, then ε also is small even if the target polarization does vary. One would expect, therefore, significant deviations from the lowest order approximation for the asymmetry if it is large and if the target polarization varies widely.

The expression for the zeroth approximation is presented in its simplest form here. It is, in practice, complicated by the fact that N_i must be determined from data which has some non-elastic background associated with it. The details of such a calculation have been given elsewhere and will not be included here.[22]

V. RESULTS AND DISCUSSION

The results for the asymmetry as a function of four-momentum transfer u are shown in Fig. 14 and tabulated in Table 1. The errors given are those due to counting statistics alone. The error due to uncertainty in the background subtraction is negligible in comparison. Checks of the consistency of our various monitors along with comparisons of the data from various periods during the data taking indicate that systematic errors, such as instabilities of our monitors and detectors, are also negligible. The only other significant source of error is due to uncertainly in the measurement of the target polarization. Our estimate of this error[23] gives rise to an overall normalization factor of (1 ± 0.05).

The curve shown on each of the graphs in Fig. 14 is not the result of any theory but is just the function $A(-u) = -0.5 \sqrt{-u}/M_p$, where M_p is the mass of the proton. The significance of the fact that this function is a good representation of the data is obscure. The sign convention for A corresponds to having the direction of the normal to the scattering plane be that of the vector product of the incident neutron momentum and the outgoing neutron momentum. The general features of the data are that it is significantly different from zero at most points (except, of course, very near u = 0) and that the sign of the asymmetry is consistently negative. In particular, there is no indication that the asymmetry passes through zero with increasing $|u|$ at any of the energies studied. There also seems to be little energy dependence at fixed u from a neutron momentum P_n of $2 \leq P_n \leq 5.5$ GeV/c.

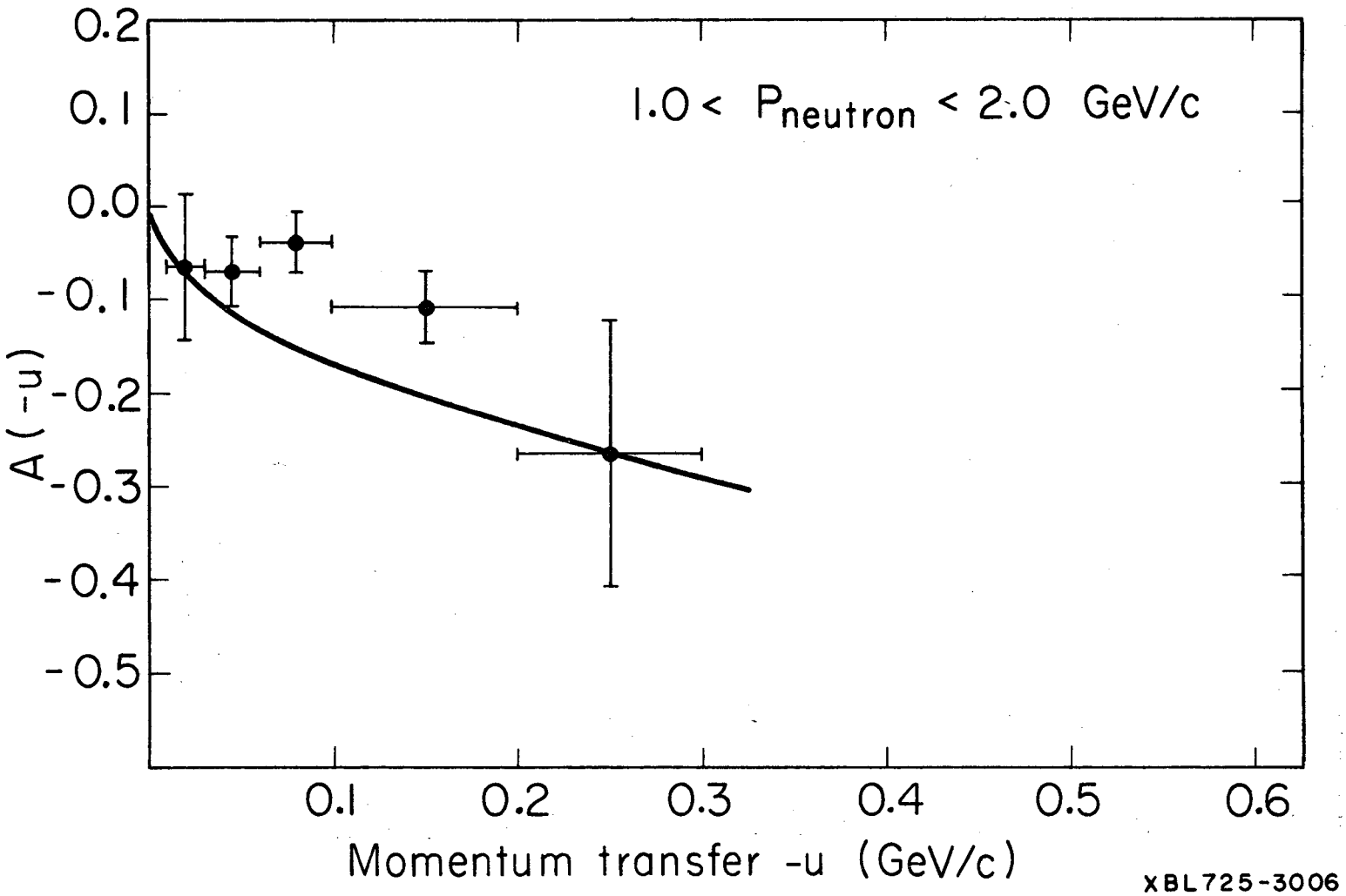

Fig. 14a. Asymmetry in np → pn with a Polarized Target at the Indicated Momenta.

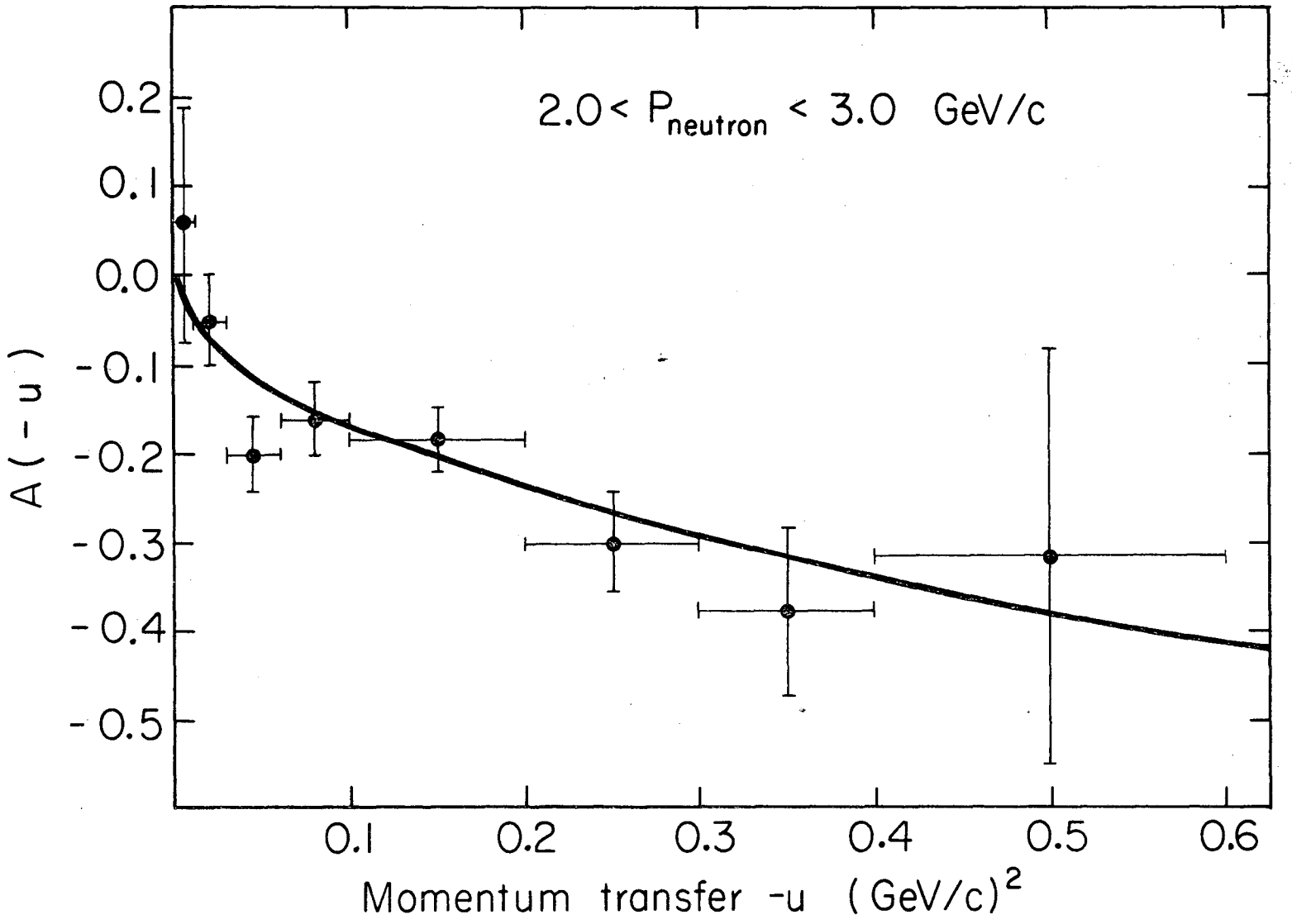

Fig. 14b. Asymmetry in np → pn with a Polarized Target at the Indicated Momenta.

XBL725-3005

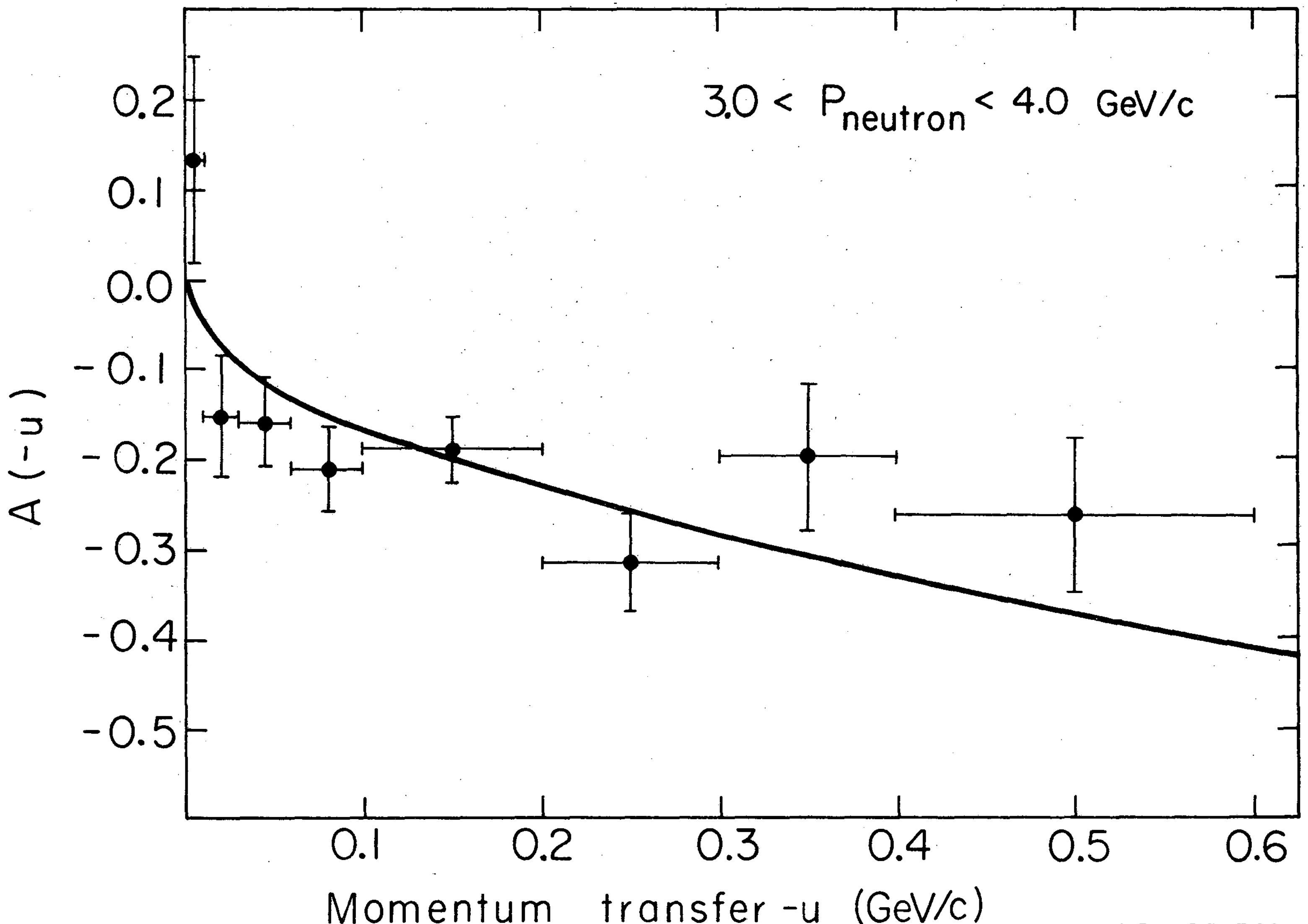

Fig. 14c. Asymmetry in np → pn with a Polarized Target at the Indicated Momenta.

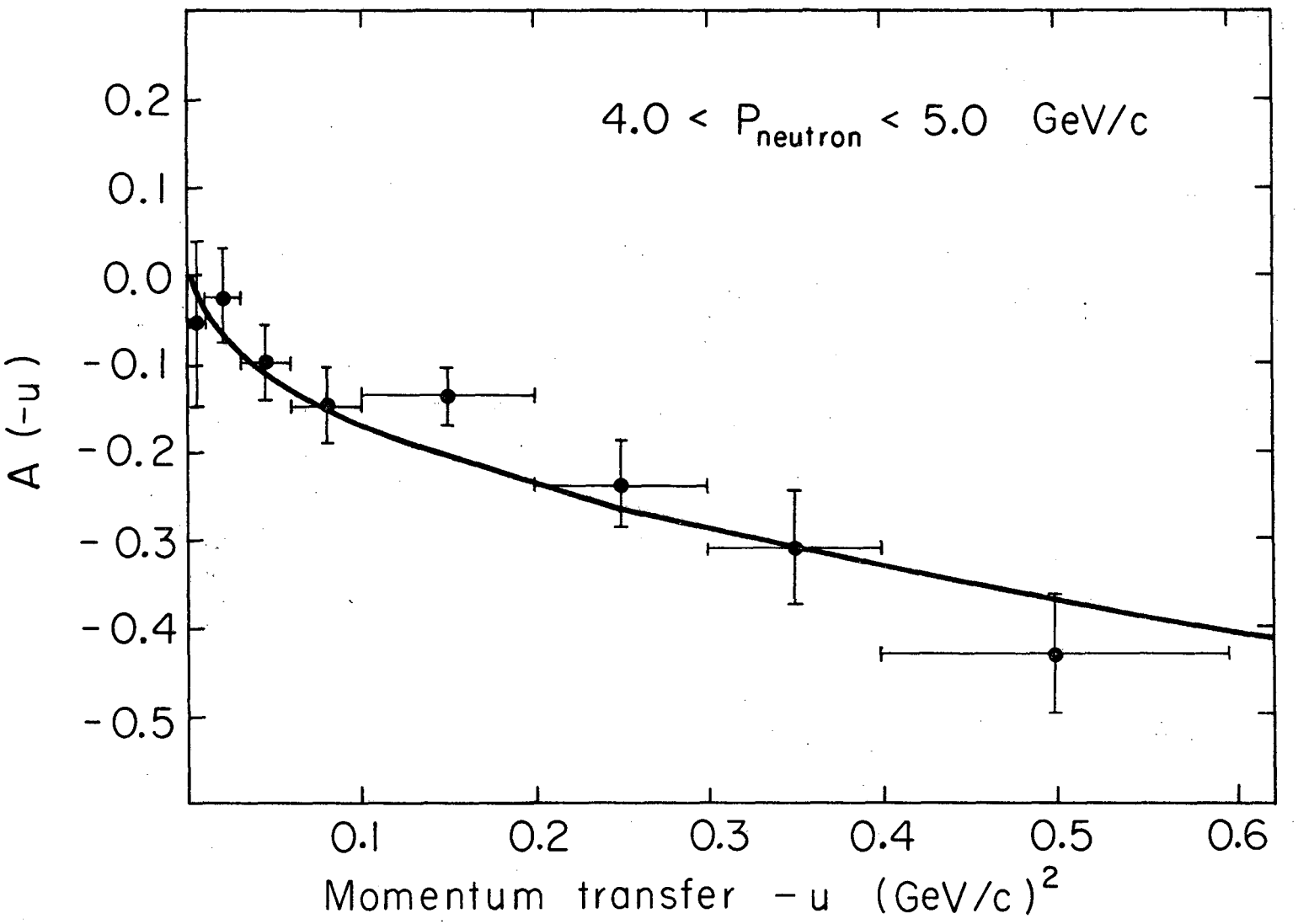

Fig. 14d. Asymmetry in np → pn with a Polarized Target at the Indicated Momenta.

XBL725-3003

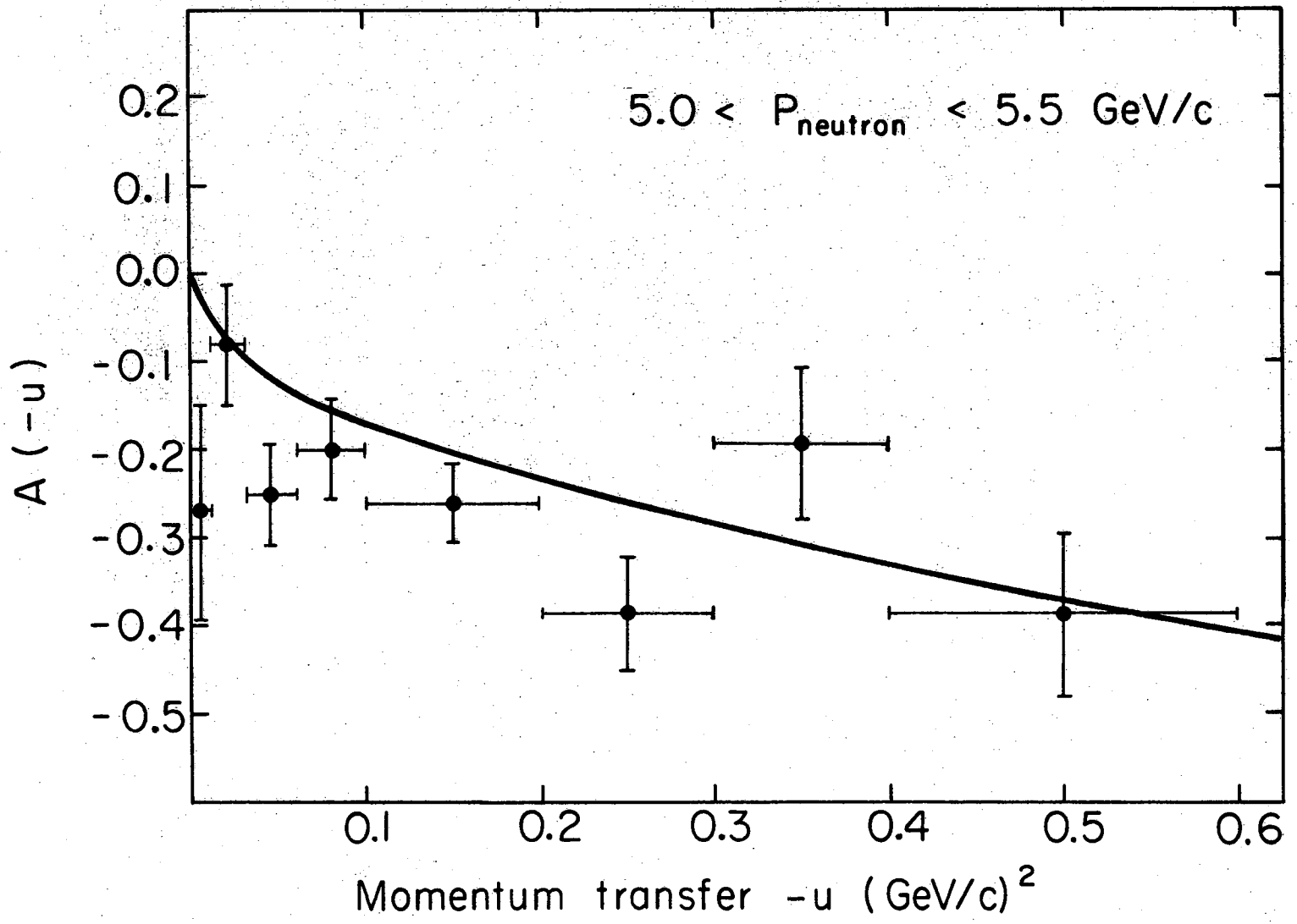

Fig. 14e. Asymmetry in np → pn with a Polarized Target at the Indicated Momenta.

XBL725-3002

The experiment of Cheng et al.[9] which measured np polarization at kinetic energies of 300-700 MeV obtained data at their highest energy (which corresponds to a neutron momentum of 1.34 GeV/c) which agrees with our data at 1.5 GeV/c. If one looks at the Cheng data as a function of u at increasing incident neutron momenta, an intriguing pattern emerges. The data rises to a maximum at a value of u (u_{max}) which increases with energy (their data, at all energies, have maxima at a center of mass angle of about 110°). The maximum values also seem to increase slightly with energy. Below u_{max} the data appear consistent with our simple $\frac{1}{2}\sqrt{-u}/M_p$ parameterization; while above it, of course, they deviate from this simple function.

How do we interpret all of this? Suppose we consider a Regge pole model in which we consider only the π, ρ, and A_2 trajectories. This is a simple-minded model, and would probably not even do a good job of fitting the cross-section, but by examining it to see where it breaks down perhaps we can gain a little insight into what has to be done to improve things. Recall that we have already shown that the π cannot contribute to the quantity $I_0A = \text{Im}\ \phi_5(\phi_1 + \phi_2 + \phi_3 - \phi_4)^*$ so that we are left with the ρ and A_2 trajectories. From Muzinich[14] we have for each of the two trajectories i (ignoring isospin which only multiplies the result by a constant):

$$\phi_1^i = \phi_4^i = -\frac{\pi}{4E \sin \pi \alpha_i} F_1^i \left(\frac{s}{s_0}\right)^{\alpha_i} (1 + \S_i\, e^{i\pi})^{\alpha_i}$$

$$\phi_2^i = \phi_3^i = \frac{\pi}{4E \sin \pi \alpha_i} F_2^i \left(\frac{s}{s_0}\right)^{\alpha_i} (1 + \S_i e^{i\pi\alpha_i})$$

$$\phi_5^i = \frac{\pi}{4m \sin \pi \alpha_i} \frac{(ut)^{1/2}}{4p^2} F_5^i \left(\frac{s}{s_0}\right)^{\alpha_i} (1 + \S_i e^{i\pi\alpha_i})$$

where F_1^i, F_2^i, F_5^i are unknown functions of u, α_i is the trajectory function (also a function of u) and $\S_i$ the signature factor. With only ρ and A_2 we have

$$I_0 A = 2 \text{ Im } (\phi_5^\rho + \phi_5^{A_2}) (\phi_1^\rho + \phi_1^{A_2} + \phi_2^\rho + \phi_2^{A_2})^*$$

The above simplification of the original expression does not hold for arbitrary trajectories.

The basic problem in this whole game is to find out what the F's and α's are. The trajectories for the ρ and A_2 seem to be very close to each other and we might therefore be tempted to invoke the concept of exchange degeneracy, which in its strongest form states that $\alpha_\rho = \alpha_{A_2}$ and $F_j^\rho = F_j^{A_2}$ (j = 1, 2, 5). Now if we assume that the F's are all real, then, since $\S_\rho = -1$ and $\S_{A_2} = +1$, $\phi_j = \phi_j^\rho + \phi_j^{A_2}$ (j = 1, 2, 5) are all real functions so that $I_0 A$ vanishes. This means that A vanishes. A naive exchange degenerate model using the ρ and A_2, therefore, predicts no asymmetry. If we now relax the condition that $F_j^\rho = F_j^{A_2}$, we can get something similar to a model of Arnold and Logan.[24] Their model agrees with the data for $|u| < 0.3$, however they predict that the sign of the asymmetry should change at $u \sim -0.5$ and we see no evidence for this cross-over.

The zero predicted in the asymmetry at u = -0.5 occurs because, assuming weak exchange degeneracy, both α_ρ and α_{A_2} vanish at the same place so that all amplitudes are purely real there. Therefore the

asymmetry vanishes. More general models involving only ρ and A_2 exchange should also show some strange behavior near the point $u \tilde{=} -0.6$, since at that point the helicity flip contribution of the ρ to the amplitude must vanish for kinematic reasons. Fits to the differential cross-sections for the reactions $\pi^- p \to \pi^0 n$ and $\pi^- p \to \eta n$ indicated that the residues for the helicity flip contributions for ρ and A_2 are large while the non-flip contributions are small.[25] Therefore the contribution from the ρ flip A_2 non-flip interference should be comparable to that from the A_2 flip ρ non-flip interference away from the region where the ρ flip contributions vanishes. Near $u \cong 0.6$, however, the ρ flip contribution varies rapidly, so that if only the ρ and A_2 were involved we would expect a rapid variation in the asymmetry. Obviously the data indicate that something else is going on.

There have recently been a number of attempts to use cut models to fit the asymmetry. Froyland and Winbow[26] compare two cut models, one called the mixed model and the other the Michigan model.[27] They find that while both models can approximate the behavior of the $np \to pn$ and $\bar{p}p \to \bar{n}n$ differential cross-sections, neither is able to reproduce the asymmetry. The mixed model gives the wrong sign while the Michigan model, which looks fine for small values of $|u|$, predicts too small an asymmetry as $|u|$ increases.

Another absorption model (usually called the hybrid model) used by Blackmon and Goldstein[28] to fit the $np \to pn$ differential cross-section, also fails to reproduce the asymmetry. A recent modification of that model by Manesis,[29] which involves the use of two ad-hoc poles in addition

to the Pomeron (and 90° out of phase with it) in the absorptive prescription, is able to generate non-vanishing asymmetries. These predictions, while they have the right sign, are not very good representations of the data.

Looking at the expressions for the ϕ's we see that the $\sqrt{-u}$ behavior is not totally mysterious since ϕ_5 contains a kinematical factor $\sqrt{-u}$. This factor $\sqrt{-u}$ is proportional to the sine of the center of mass scattering angle for small u. It is still unclear, at least to the author, why this behavior persists to such large values of u. $A = I_0 A/I_0$ should have this behavior for small u since I_0, outside the very forward peak region, varies slowly, but it is strange that higher order terms in u do not seem to contribute to A out to $u = -0.6$. We should note in this connection that a recent experiment has been done to measure the asymmetry in π^+ photoproduction,[30] a reaction which is thought to proceed by a similar mechanism to backward np scattering.[27,31] At 5 GeV incident photon energy the asymmetry, though of opposite sign to ours, also varies as the square root of the four-momentum transfer out to a momentum transfer of about -0.6. From this discussion it appears that two conclusions emerge. First, the asymmetry measurements provide a difficult and detailed test for Regge models and secondly there appears to be increasing evidence linking np backward scattering with charged pion photoproduction. If this connection with the photoproduction reaction is real, then it would be interesting to measure the asymmetry in $np \to pn$ at quite high energies, since for the photoproduction, the asymmetries were still very large when the incident photon had an energy of 16 GeV.

Table I

Asymmetry in np → pn with a polarized proton target versus momentum transfer -u from 1.0 - 5.5 GeV/c. Errors shown are statistical only, and do not include a possible correction factor of (1.00 ± 0.05) to account for uncertainty in the target polarization.

Neutron Momentum (GeV/c)	Momentum Transfer $(GeV/c)^2$	Asymmetry
1.0 - 2.0	.01 - .03	-.063 ± .078
	.03 - .06	-.068 ± .036
	.06 - .1	-.036 ± .032
	.1 - .2	-.107 ± .038
	.2 - .3	-.264 ± .143
2.0 - 3.0	0.0 - .01	.059 ± .129
	.01 - .03	-.049 ± .052
	.03 - .06	-.200 ± .043
	.06 - .1	-.160 ± .041
	.1 - .2	-.182 ± .038
	.2 - .3	-.298 ± .058
	.3 - .4	-.378 ± .095
	.4 - .6	-.314 ± .235
3.0 - 4.0	0.0 - .01	.132 ± .115
	.01 - .03	-.153 ± .066
	.03 - .06	-.161 ± .048
	.06 - .1	-.212 ± .046
	.1 - .2	-.189 ± .037
	.2 - .3	-.315 ± .055
	.3 - .4	-.197 ± .080
	.4 - .6	-.263 ± .085

(Continued on next page)

Table I (cont.)

Neutron Momentum (GeV/c)	Momentum Transfer $(GeV/c)^2$	Asymmetry
4.0 - 5.0	0.0 - .01	-.053 ± .095
	.01 - .03	-.023 ± .056
	.03 - .06	-.098 ± .044
	.06 - .1	-.146 ± .043
	.1 - .2	-.136 ± .033
	.2 - .3	-.237 ± .050
	.3 - .4	-.309 ± .064
	.4 - .6	-.430 ± .068
5.0 - 5.5	0.0 - .01	-.268 ± .121
	.01 - .03	-.081 ± .067
	.03 - .06	-.251 ± .058
	.06 - .1	-.200 ± .056
	.1 - .2	-.260 ± .044
	.2 - .3	-.384 ± .065
	.3 - .4	-.193 ± .085
	.4 - .6	-.385 ± .092

Acknowledgments

It is a pleasure to thank Professor Owen Chamberlain, Professor Herbert Steiner and Professor Gilbert Shapiro for their guidance and encouragement throughout the course of my graduate studies, and for their efforts in the design and execution of this experiment.

I would like to thank Professor Michael Longo of the University of Michigan for his suggestion of and collaboration on the experiment described in this thesis. Also I would like to acknowledge the cooperation and hard work of Professor Howard Weisberg of the University of Pennsylvania.

My fellow graduate students deserve much of the credit for the successful completion of this experiment. Dr. Stephen Rock deserves credit for the successful operation of the neutron counters and their associated circuitry, Dr. Charles Morehouse for the polarized target readout and computer programming, Dr. Thomas Powell, Stephen Shannon, and William Gorn deserve special thanks for the long hours spent running the experiment. All are especially thanked for being good people with whom to work and for their salutory effects on my sanity.

Raymond Z. Fuzesy deserves a book of acknowledgments all his own; however, I will just say that I would like to thank him for being a superb technician, for his efforts to teach me the

machinists trade, and for helping to keep my car together for the past six years.

Finally, special words of thanks to Rosemary Fowell, Genece Hoskin, and Suzie Sayre who have cheerfully done the typing of the many and varied revisions of this thesis.

FOOTNOTES AND REFERENCES

1. I apologize to the reader who is confused by my reference to this reaction as np backward scattering rather than np forward charge exchange. Most theoretical papers which consider the reaction prefer to think of it as forward charge exchange scattering, perhaps because they don't wish to work with u channel amplitudes. I prefer to call it backward scattering so that those experimenters who look at the np reaction for intermediate center-of-mass angles will have a consistent framework in which to compare their results with the forward and backward measurements. Since I don't think that anyone can define exactly at what value of u to stop calling backward np scattering np charge exchange, I prefer not to start calling it that.

2. J. L. Friedes, H. Palevsky, R. L. Stearns, and R. J. Sutter, Phys. Rev. Letters 15, 38 (1965).

3. G. Manning, A. G. Parham, J. D. Jafar, H. B. van der Raag, D. H. Reading, D. G. Ryan, B. D. Jones, J. Malos, and N. H. Lipman, Nuovo Cimento 41, 167 (1966).

4. R. E. Mischke, P. F. Shepard, and T. J. Devlin, Phys. Rev. Letters 23, 542 (1969).

   P. F. Shepard, T. J. Devlin, R. E. Mischke, and J. Solomon, Princeton-Pennsylvania Accelerator Report PPAR 10 (1969).

5. J. Engler, K. Horn, F. Monnig, P. Schludecker, W. Schmidt-Parzefall, H. Schopper, P. Sievers, H. Ullrich, R. Hartung, K. Runge, and Yu. Galaktionov, Phys. Letters 34B, 528 (1971).

E. L. Miller, Mark Elfield, N. W. Reay, N. R. Stanton, M. A. Abolins, M. T. Lin and K. W. Edwards, Phys. Rev. Letters 26, 984 (1971).

6. R. Wilson, Ann. Phys. (N.Y.) 32, 193 (1965).
7. A. M. Boyarski, F. Bulos, W. Busza, R. Diebold, S. D. Ecklund, G. E. Fischer, J. R. Rees, and B. Richter, Phys. Rev. Letters 20, 300 (1968).
8. B. M. Golovin, V. P. Dzhelepov, V. S. Nadezhdin and V. I. Satarov, J. Exptl. Theoret. Phys. 36 433 (1959); (English translation) Sov. Phys. JETP 9, 302 (1959).
9. D. Cheng, B. Macdonald, J. A. Helland and P. M. Ogden, Phys. Rev. 163, 1470 (1967).
10. E. M. Henley and I. J. Muzinich, Phys. Rev. 136 B 1783 (1964), G. A. Ringland and R. J. N. Phillips, Phys. Lett. 12 62 (1964). L. Durand III and Y. T. Chiu, Phys. Rev. 137 B 1530 (1965). I should note that Miller et al.[5] report a small shoulder near $|U| = .04$, but it is not nearly the magnitude predicted by these models.
11. N. Byers, Phys. Rev. 156, 1703 (1967).
12. M. Jacob and G. C. Wick, Ann. Phys. (N.Y.) 7, 404 (1959).
13. M. L. Goldberger, M. T. Grisaru, S. W. MacDowell, and D. Y. Wong, Phys. Rev. 120, 2250 (1960).
14. I. J. Muzinich, Phys. Rev. 130, 1571 (1963).
15. R. J. N. Phillips, Nucl. Phys. B2, 394 (1967).
16. K. Huang and I. J. Muzinich, Phys. Rev. 164, 1726 (1967). F. Arbab and J. W. Dash, Phys. Rev. 163, 1603 (1967).
17. M. LeBellac, Phys. Lett. 25B, 524 (1967).

18. M. Aderholz, J. Bartsch, M. Deutschmann, G. Kraus, R. Speth, C. Grote, K. Lanius, S. Nowak, M. Walter, H. Bottcher, T. Byer, V. T. Cocconi, J. D. Hansen, G. Kellner, A. Mihul, D. R. O. Morrison, V. I. Moskalev, and H. Tofte, Phys. Lett. 27B, 174 (1968).

19. F. Henyey, G. L. Kane, J. Pumpkin and M. H. Ross, Phys. Rev. 182, 1579 (1969); A. B. Kaidalov and B. M. Karnakov, Phys. Letters, 29B, 372 (1969).

20. G. Shapiro in Progr. in Nucl. Techn. and Instrumentation, Vol. I, p. 173 (North Holland Publishing Company, Amsterdam, 1964).
M. Borghini, Ecole Internationale de la Physique des Particules Elementaires, Herceg Novi, Yugoslavia (1968).
C. D. Jeffries, Dynamic Nuclear Orientation (Interscience Publishers Inc., New York, 1963).

21. Q. A. Kerns, H. W. Miller and A. H. Wolverton, Chamberlain Proton Spin Resonance RF System 1260, UCRL-17548, Vol. I., Vol. II (unpublished).

22. C. H. Johnson, Jr., Measurement of the Polarization Parameters in Proton-Proton Scattering from 1.7 to 6.1 BeV, UCRL 16070 (unpublished).

23. C. C. Morehouse, Photoproduction of π^+ Mesons from a Polarized Proton Target at 5 and 16 GeV (Ph.D. Thesis), UCRL 19897 (unpublished), p. 65.

24. R. C. Arnold and R. K. Logan, Phys. Rev. 177, 2318 (1969).

25. F. Arbab and C. B. Chiu, Phys. Rev. 147, 1045 (1966).
R. J. N. Phillips, Nucl. Phys. B1, 572 (1967).

26. J. Froyland and G. A. Winbow, Nucl. Phys. B35, 351 (1971)

27. G. L. Kane, F. Henyey, D. R. Richards, M. Ross and G. Williamson, Phys. Rev. Lett. 25, 1519 (1970).

28. M. L. Blackmon and G. R. Goldstein, Phys. Rev. D1, 2675 (1970).

29. E. K. Manesis, High Energy Nucleon-Nucleon Charge Exchange Scattering in a Weak Cut Model, ANL/HEP 7214 (unpublished).

30. C. C. Morehouse, M. Borghini, O. Chamberlain, R. Fuzesy, W. Gorn, T. Powell, P. Robrish, S. Rock, S. Shannon, G. Shapiro, H. Weisberg, A. Boyarski, S. Ecklund, Y. Murata, B. Richter, R. Siemann and R. Diebold, Phys. Rev. Lett. 25, 835 (1970).

31. Loyal Durand III, Phys. Rev. Lett. 12, 1345 (1967).

R. Wilson, Comments on Nuclear and Particle Physics, 2, 41 (1968).

TECHNICAL INFORMATION DIVISION
LAWRENCE BERKELEY LABORATORY
UNIVERSITY OF CALIFORNIA
BERKELEY, CALIFORNIA 94720